



# LUND UNIVERSITY

## alpha-synuclein: amyloid fibrils and interactions with lipid membranes

Dubackic, Marija

2021

[Link to publication](#)

*Citation for published version (APA):*

Dubackic, M. (2021). *alpha-synuclein: amyloid fibrils and interactions with lipid membranes*. Lund University.

*Total number of authors:*

1

### General rights

Unless other specific re-use rights are stated the following general rights apply:

Copyright and moral rights for the publications made accessible in the public portal are retained by the authors and/or other copyright owners and it is a condition of accessing publications that users recognise and abide by the legal requirements associated with these rights.

- Users may download and print one copy of any publication from the public portal for the purpose of private study or research.
- You may not further distribute the material or use it for any profit-making activity or commercial gain
- You may freely distribute the URL identifying the publication in the public portal

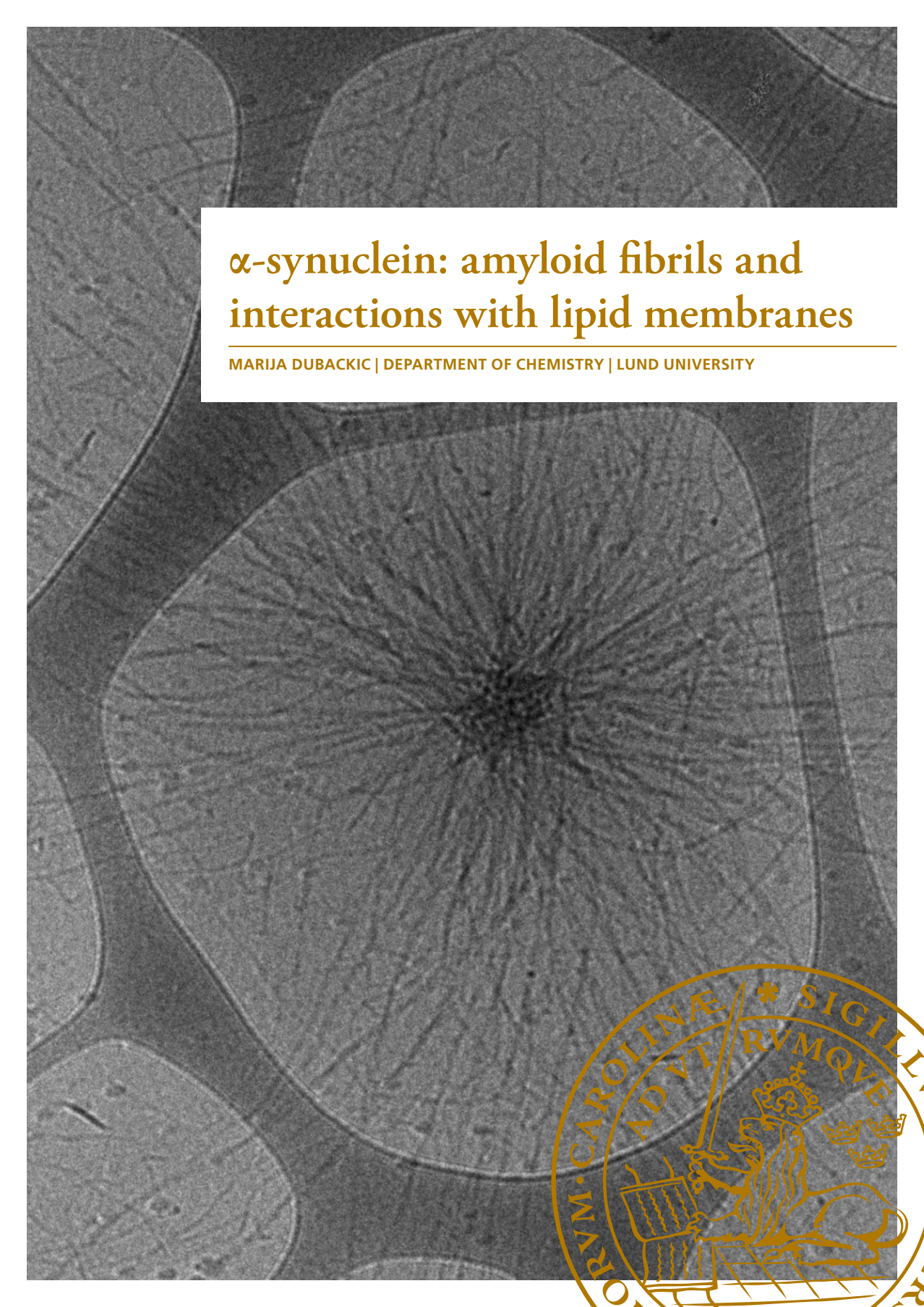
Read more about Creative commons licenses: <https://creativecommons.org/licenses/>

### Take down policy

If you believe that this document breaches copyright please contact us providing details, and we will remove access to the work immediately and investigate your claim.

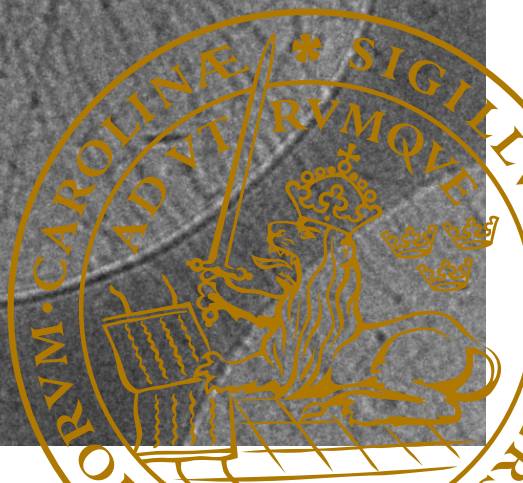
LUND UNIVERSITY

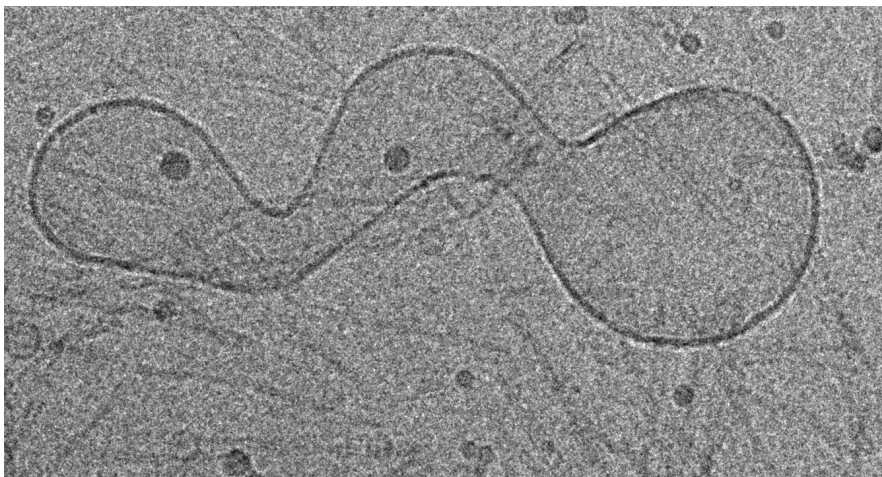
PO Box 117  
221 00 Lund  
+46 46-222 00 00

A grayscale electron micrograph showing numerous amyloid fibrils. The fibrils are thin, thread-like structures that form a dense, interconnected network. Some larger, circular structures are visible, possibly representing amyloid plaques or aggregates. The overall appearance is that of a complex, fibrous material.

# $\alpha$ -synuclein: amyloid fibrils and interactions with lipid membranes

MARIJA DUBACKIC | DEPARTMENT OF CHEMISTRY | LUND UNIVERSITY





ISBN: 978-91-7422-840-3

Physical Chemistry  
Faculty of Science  
Lund University



$\alpha$ -synuclein: amyloid fibrils and interactions with lipid membranes



# $\alpha$ -synuclein: amyloid fibrils and interactions with lipid membranes

by Marija Dubackic



**LUND**  
UNIVERSITY

DOCTORAL DISSERTATION

by due permission of the Faculty of Science, Lund University, Sweden.

To be defended on Thursday, the 16th of December 2021 at 13:00 in Lecture hall A at the  
Department of Chemistry, Lund University.

*Faculty opponent*

Prof Raffaele Mezzenga  
ETH, Zurich, Switzerland

Organization <b>LUND UNIVERSITY</b> Department of Chemistry Box 124 SE-221 00 LUND Sweden		Document name <b>DOCTORAL DISSERTATION</b>	
Author(s) Marija Dubackic		Date of disputation 2021-12-16	
		Sponsoring organization Funding information could go here.	
Title and subtitle <b><math>\alpha</math>-synuclein: amyloid fibrils and interactions with lipid membranes:</b>			
Abstract The second most common neurodegenerative disease, Parkinson's disease, is linked with an amyloid forming protein, $\alpha$ -synuclein. Hallmarks of Parkinson's disease are progressive loss of dopaminergic neurons and accumulation of intraneuronal inclusions termed Lewy bodies. Major components of Lewy bodies are amyloid fibrils formed by $\alpha$ -synuclein and various lipids and cell organelles. In this thesis, we investigated the interaction of $\alpha$ -synuclein and different model lipid membranes. The main techniques have been small-angle neutron scattering (SANS) and small-angle X-ray scattering (SAXS). We focused on the structure of aSyn fibrils and model lipid membranes, both alone and when in the presence of each other. The investigations were performed when the protein was present both in its monomeric and fibrillar form. We also studied fibril formation process in the presence of model membranes and followed the effect it has on the membrane structure, as well as the effect membranes have on the structure of mature fibrils. Finally, we investigated arrangement of colloiddally unstable $\alpha$ -synuclein fibrils and their interaction with various lipid membranes. We learned that interaction of monomeric $\alpha$ -synuclein and lipid disc micelles results in a major deformation of the disc shape, but that the partial recovery is possible due to the desorption of monomers and their incorporation into amyloid fibrils. We also learned that the fibril formation can cause vesicle fusion. The presence of model membranes during the fibril formation has no effect on the cross-sectional size and structure of fibrils, nor is there any observable incorporation of lipid molecules into the mature fibrils. The colloiddally unstable $\alpha$ -synuclein fibrils arrange into mass clusters, independent on the presence of different lipid vesicles, and this arrangement is reproduced with a simple rigid-rod cluster model.			
Key words $\alpha$ -synuclein, model lipid membranes, amyloid fibrils, Parkinson's disease, Lewy bodies, SANS, SAXS			
Classification system and/or index terms (if any)			
Supplementary bibliographical information		Language English	
ISSN and key title		ISBN 978-91-7422-840-3 (print) 978-91-7422-841-0 (pdf)	
Recipient's notes		Number of pages 198	Price
		Security classification	

I, the undersigned, being the copyright owner of the abstract of the above-mentioned dissertation, hereby grant to all reference sources the permission to publish and disseminate the abstract of the above-mentioned dissertation.

Signature



Date 2021-11-05

# $\alpha$ -synuclein: amyloid fibrils and interactions with lipid membranes

by Marija Dubackic



**LUND**  
UNIVERSITY



This doctoral thesis is constructed as a summary of research papers and consists of two parts. An introductory text puts the research work into context and summarises the main conclusions of the papers. Then, the research publications themselves are reproduced. The research papers may either have been already published or are manuscripts at various stages.

**Cover photo front:** Cryo-TEM image of  $\alpha$ -synuclein fibrils formed at pH 5.5  
**Cover illustration back:** Cryo-TEM image of a possible artefact

© Marija Dubackic 2021

Faculty of Science, Department of Chemistry, Division of Physical Chemistry

ISBN: 978-91-7422-840-3 (print)

ISBN: 978-91-7422-841-0 (pdf)

Printed in Sweden by Media-Tryck, Lund University, Lund 2021



Media-Tryck is a Nordic Swan Ecolabel certified provider of printed material. Read more about our environmental work at [www.mediatryck.lu.se](http://www.mediatryck.lu.se)

Printed matter  
3041 0903

**MADE IN SWEDEN** 

*To my mother*





# Table of Contents

Acknowledgments . . . . .	iv
Popular summary in English . . . . .	vi
Populärvetenskaplig Sammanfattning . . . . .	viii
List of Publications . . . . .	x
Author Contributions . . . . .	xi
Abbreviations . . . . .	xii
<b>Prologue</b>	<b>1</b>
<b>1 Introduction</b>	<b>5</b>
1.1 Protein folding versus amyloid fibril formation . . . . .	6
1.2 Amyloid fibrils and disease pathogeneses . . . . .	9
1.3 $\alpha$ -synuclein . . . . .	10
1.4 $\alpha$ -synuclein and lipid membranes . . . . .	11
<b>2 Materials</b>	<b>13</b>
2.1 $\alpha$ -synuclein expression and purification . . . . .	14
2.2 Model membrane preparation . . . . .	15
2.3 Fibril formation . . . . .	15
<b>3 Methods</b>	<b>17</b>
3.1 Scattering . . . . .	18
3.2 Nuclear magnetic resonance . . . . .	27
3.3 Cryogenic transmission electron microscopy . . . . .	29
3.4 Circular dichroism spectroscopy . . . . .	29
<b>4 <math>\alpha</math>-synuclein: amyloid fibrils and interactions with lipid membranes</b>	<b>31</b>
4.1 Part I: aSyn–membrane interactions and co–assembly formation . . . . .	32
4.2 Part II: Arrangements of colloiddally unstable aSyn fibrils . . . . .	46
<b>5 Epilogue</b>	<b>53</b>
<b>Scientific Publications</b>	<b>63</b>

## Acknowledgments

I would like to start by expressing my deepest gratitude to my supervisors, **Ulf, Sara** and **Emma**. Thank you for giving me the opportunity to pursue my PhD under your guidance.

**Ulf**, you have always been a great support! You are such a kind person who cares about the wellbeing of your students and I couldn't have asked for a better supervisor. I have learned so much from you. Thank you!

**Sara**, it has been a great honour to be a part of your group! I am grateful for all the help and input I got from you.

**Emma**, thank you for all the guidance and constructive comments you provided me with whenever we would talk.

I would now like to express my gratitude to my closest colleagues. **Axel**, thank you for helping me with countless things countless times. **Vero**, thank you for getting me familiarised with the lab work and for all the beamtimes and all the fun we had together. And to some of many of my amazing colleagues, **Dev, Vika, Erika, Jon, Luigi, Kasia, Simon, Tommy** thank you for various constructive inputs, laughs and good memories we shared. Special thanks to the Fkem administration: **Helena, Maria L, Maria S** and **Chris** for always being there and ready to help.

I would then like to thank to my graduate school **SwedNESS** for funding this amazing journey called PhD studies. It has provided me with great knowledge of neutron scattering, allowed me to travel the world and to connect with great people, especially my comrades **Zuza** and **Prabhat**. Thank you for being such good friends.

**Yun Liu**, thank you for being my host during my 3-month stay at NCNR and being such a knowledgeable and kind supervisor.

I would also like to thank to my elected family, the Norsemen crew. **Albert, Eliška, Elias, Isak, Julie, Fabio** and **Nadja**, thank you for being such good people and friends and for all the fun we had and are going to have. Surviving the pandemic with you was a piece of cake!

I am also truly grateful to my original family! To my relatives in Sweden, thank you for making me feel like home here. **Tata**, thank you for always being there for me and for inspiring me to pursue a life of a scientist. **Veljo**, thank you for being the best brother that I can always rely on.

To my soulmate, **Isak**! Your support means the world to me and during these past

months that I have been working on this book, it was priceless and absolutely necessary. I am so grateful to have you by my side!

## Popular summary in English

Parkinson's disease (PD) is the second most common neurodegenerative disease, and it was first described by James Parkinson in 1817. The cardinal symptoms of PD include movement disorders such as tremor at rest, rigidity, slowness of movement, reduction in movement amplitude and absence of voluntary movement. PD is characterised by progressive loss of dopaminergic neurones in the midbrain region called substantia nigra pars compacta and the presence of intraneuronal inclusions called Lewy bodies (LBs). An ongoing challenge with detecting and treating PD is that its symptoms usually do not manifest before ca. 70% of dopaminergic neurons have already been lost, and there are currently no methods to detect LBs in living patients.

PD belongs to a specific group of diseases termed amyloidoses. Amyloidoses are conditions that are related to the misfolding and aggregation of specific proteins. These aggregates are well structured, long fibrils, called amyloid fibrils. Some other diseases included in the group of amyloidoses are Alzheimer's disease, diabetes type II and Huntington's disease.

The amyloid forming protein implicated with PD is  $\alpha$ -synuclein (aSyn). The exact way in which aSyn is involved with PD remains elusive. Mutations and duplications in the gene for aSyn are known to cause hereditary PD. Moreover, it has been demonstrated that aSyn fibrils are the main component of LBs, together with various lipid membrane structures. There are suggestions that the cell death related to PD is due to the interaction of aSyn and cell membranes. One of the proposed mechanisms is that the cell membranes get disrupted during the formation of aSyn fibrils through extraction of lipid molecules from the membrane.

The biological function of aSyn is not well understood either. However, it has been suggested that it involves an interaction of aSyn with membrane lipids in the synapses of neurones and that this helps regulate essential aspects of brain function.

In order to gain more insight into how aSyn interacts with lipid membranes, we have in this thesis performed various experiments on model mixtures of lipids and the protein. We also followed the formation of amyloid fibrils in the presence of model membranes, and we investigated the arrangement of aSyn fibrils into clusters that resemble the fibrillar networks found within LBs and how such clusters interact with lipids.

We learned that aSyn adsorption onto lipid membranes depends on the amount of charged lipids in the membranes. We also demonstrated that when aSyn fibrils are formed in the presence of lipid disc micelles and lipid vesicles, it can lead to reversible modifications in morphologies in the former case and vesicle fusion in the latter

case. Further on, we found that the presence of vesicles during the fibril formation did not result in the extraction of lipids from the vesicles nor any lipid incorporation into fibrils. We also analysed the arrangement of aSyn fibrils that resemble the fibrillar network found in LBs and learned that they form so-called mass fractals due to predominant attractive fibril-fibril interactions.

The use of these simpler model systems allowed us to answer questions that would be impractical to pursue in an *in-vivo* context and could help inform research onto the role of aSyn in health and disease.



## Populärvetenskaplig Sammanfattning

Parkinsons sjukdom (PD) är den vanligaste neurodegenerativa sjukdomen och beskrevs först av James Parkinson 1817. Symptomen inkluderar störningar i rörelser såsom vilotremor, stelhet, långsamma rörelser, instabil hållning och problem med att initiera rörelser. PD karakteriseras av en fortskridande degeneration av dopaminerga nervceller i substantia nigra pars compacta samt förekomsten av abnorma intraneuronala inklusioner, kända som Lewykroppar. En av utmaningarna vid behandling och diagnostisering av PD är att de karaktäristiska motor symptomen inte uppkommer förrän ungefär 70% av de dopaminerga nervcellerna har dött. Dessutom saknas fortfarande metoder för att upptäcka Lewykroppar i levande patienter.

PD tillhör en grupp sjukdomar som kallas amyloidoser. Amyloidoser är tillstånd som orsakas av en abnormal ansamling och aggregering av felveckade proteiner. Dessa proteinaggregat, så kallade amyloider, är välstrukturerade och långa fibrer. Exempel på amyloida sjukdomar är bland annat, Alzheimers sjukdom, diabetes typ 2 och Huntingtons sjukdom.

Det amyloida protein som är associerat med PD kallas alfa-synuclein. Det är ännu okänt exakt hur alfa-synuclein orsakar PD men man har visat att det är en av huvudkomponenterna i Lewykroppar, tillsammans med olika lipidstrukturer. Dessutom är mutationer och duplikationer i genen för alfa-synuclein kopplade till ärftlig PD. En av de föreslagna mekanismerna för celledöd i PD är att alfa-synuclein interagerar med membranet och att det vid aggregering leder en lipidextraktion med permeabilisering av membranet som följd.

Alfa-synucleins biologiska roll är ännu inte helt klarlagd, det spekuleras dock alfa-synucleins interaktion med lipidmembran vid synapser i nervceller reglerar viktiga funktioner i hjärnan.

För att nå insikt i hur alfa-synuclein interagerar med lipider så har vi i den här tesen utfört en serie experiment på blandningar mellan alfa-synuclein och olika modellmembran. Vidare så följde vi bildandet av amyloider då alfa-synuclein får aggregera tillsammans med diverse modellvesiklar. Vi studerade dessutom hur alfa-synuclein formar kluster som liknar de fibernätverk som finns inuti Lewykroppar.

Vi upptäckte att adsorptionen av alfa-synuclein till modellmembran beror på mängden laddade lipider i dessa membran. Vidare så demonstrerade vi att alfa-synucleinsaggregering i närvaron av lipidmicellsdiskar och lipidvesiklar kan detta leda till en reversibel morfologisk förändring i det första fallet samt vesikelfusering i det andra fallet. Dessutom visade vi närvaron av vesiklar under aggregeringsprocessen varken ledde till lipidextraktion eller inkorporering av lipider i amyloiderna. Slutli-

gen så analyserade vi arrangemang av alfa-synuklein fibrer som liknar de kluster som förekommer i Lewykroppar och visar att de bildar så kallade massfraktaler genom huvudsakligen attraktiva fibrill-fibrill interaktioner.

Genom att använda dessa simplare modellsystemen har vi kunnat svara på frågor som hade varit opraktiska att ställa i in-vivo system. De resultat vi fått kan hjälpa till att informera forskning kring alfa-synukleins roll i hälsa och sjukdom.

## List of Publications

This thesis is based on the following publications, referred to by their Roman numerals:

- I  **$\alpha$ -synuclein interaction with lipid disc micelles.**  
M. Dubackic, Y. Liu, C. Hetherington, M. Haertlein, J. M. Devos, S. Linse, E. Sparr, U. Olsson  
*Manuscript*
- II  **$\alpha$ -synuclein interaction with POPC/POPS vesicles.**  
M. Dubackic, V. Lattanzi, Y. Liu, M. Haertlein, J. M. Devos, E. Sparr, S. Linse, U. Olsson  
*Manuscript*
- III **Comparing  $\alpha$ -synuclein fibrils formed in the absence and presence of a model lipid membrane: A small and wide-angle X-ray scattering study.**  
M. Dubackic, S. Linse, E. Sparr, U. Olsson  
*Submitted*
- IV **On the cluster formation of  $\alpha$ -synuclein fibrils.**  
M. Dubackic, I. Idini, V. Lattanzi, Y. Liu, A. Martel, A. Terry, M. Haertlein, J. M. Devos, A. Jackson, E. Sparr, S. Linse, U. Olsson  
*Front. Mol. Biosci. - Structural Biology* 2021, 8, 768004
- V **Lipid vesicles interactions with  $\alpha$ -synuclein fibril clusters.**  
M. Dubackic, V. Lattanzi, Y. Liu, S. Linse, E. Sparr, U. Olsson  
*Manuscript*

All papers are reproduced with permission from their respective copyright holders.

## Author Contributions

**Paper I:  $\alpha$ -synuclein interaction with lipid disc micelles.** MD conceived and designed the study together with YL, ES, SL and UO. MD performed ThT experiment. MD analysed all data. MD wrote the article with input from all co-authors.

**Paper II.  $\alpha$ -synuclein interaction with POPC/POPS vesicles.** MD conceived and designed the study together with ES, SL and UO . MD conducted CD, DLS, SAXS and SANS experiments and analysed data. MD wrote the article with input from all co-authors.

**Paper III: Comparing  $\alpha$ -synuclein fibrils formed in the absence and presence of a model lipid membrane: A small and wide-angle X-ray scattering study.** MD conceived and designed the study together with ES, SL and UO . MD conducted all experiments and analysed data. MD wrote the article with input from all co-authors.

**Paper IV: On the cluster formation of  $\alpha$ -synuclein fibrils.** MD conceived research together with II, AJ, ES, SL, UO. MD performed part of the experiments and performed computer modelling and data analysis. MD wrote the paper with input from all other co-authors.

**Paper V: Lipid vesicles interactions with  $\alpha$ -synuclein fibril clusters.** MD conceived and designed the study together with ES, SL and UO . MD conducted all experiments and performed data analysis. MD wrote the article with input from all co-authors.

## Abbreviations

AD	Alzheimer's disease
aSyn	$\alpha$ -synuclein
CD	circular dichroism
cryo-TEM	cryogenic transmission electron microscopy
DLS	dynamic light scattering
DMPC	1,2-dimyristoyl-sn-glycero-3-phosphocholine
DMPS	1,2-dimyristoyl-sn-glycero-3-phospho-L-serine
DOPC	1,2-dioleoyl-sn-glycero-3-phosphocholine
DOPS	1,2-dioleoyl-sn-glycero-3-phospho-L-serine
EM	electron microscopy
GM	ganglioside lipids
LBs	Lewy bodies
NAC	non-amyloid- $\beta$ component
NMR	nuclear magnetic resonance
PC	phosphatidylcholine
PD	Parkinson's disease
POPC	1-palmitoyl-2-oleoyl-glycero-3-phosphocholine
POPS	1-palmitoyl-2-oleoyl-sn-glycero-3-phospho-L-serine
PS	phosphatidylserine
SANS	small-angle neutron scattering
SAXS	small-angle X-ray scattering
SLD	scattering length density
ss-NMR	solid-state nuclear magnetic resonance
SUVs	small unilamellar vesicles
UV	ultra violet
WAXS	wide angle X-ray scattering



# Prologue

The objective of this thesis was to gain insight into the amyloid forming protein,  $\alpha$ -synuclein (aSyn) and its interaction with lipid membranes. Both aSyn and lipids are implicated with Parkinson's disease (PD), a neurodegenerative disease, characterised by progressive death of dopamine nerve cells in the *Substantia nigra pars compacta* and by the presence of abnormal intraneuronal inclusions called Lewy bodies (LBs). The main components of LBs are amyloid fibrils formed by aSyn and various lipids.

This thesis, is divided into two parts, associated with different overarching questions. In Part I (papers I, II and III) we focus on aSyn monomer adsorption onto model lipid membranes, and whether lipids co-assemble with aSyn in the fibril formation process. In Part II (papers IV and V) we address fibril-fibril interactions and investigate fibril cluster formation in mildly acidic conditions, also in the presence of lipids.

The main findings of this thesis can be summarized as follows:

## Part I

- **Overarching question:** What is the nature of the interaction between monomeric aSyn and lipid membranes and does the fibril formation in the presence of lipid membranes lead to a protein-lipid co-assembly formation and membrane disruption?

**Paper I:** In this paper we investigated the interaction of aSyn and lipid disc micelles.

- **Findings:** aSyn monomers adsorb onto lipid disc micelles, which results in a significant deformation of the disc shape. The deformations are happening immediately upon the mixing of aSyn monomers and lipid disc micelles. When fibrils form and consume monomers, deformed micelles recover back to their initial shape resulting in a co-existence of the deformed and recovered micelles.
- **Conclusions:** The micelle recovery can be related to the desorption of aSyn monomers from the disc surface and their incorporation in aSyn fibrils. The coexistence of both deformed and recovered micelles implies strong positive cooperativity of aSyn desorption.

**Paper II:** In this paper we investigated the interaction between aSyn and POPC/POPS vesicles. We studied how monomeric aSyn adsorbs onto vesicles, when the latter one contains different amounts of charged lipids, and how does the fibril formation process influence vesicle integrity.

- **Findings:** The adsorbed amount of aSyn onto model membranes is increasing with increasing amount of phosphatidylserine (PS). There is vesicle fusion occurring during aSyn fibril formation.
- **Conclusions:** The  $\alpha$ -helix that forms when aSyn adsorbs onto the vesicles is not dependent on the amount of charged lipids in the membranes, which implies that the adsorption is electrostatically driven process. ASyn fibril formation in the presence of vesicles results in limited vesicle fusion, where on average 3–4 initial vesicles fuse together.

**Paper III:** In this paper we investigated the potential impact of POPC/POPS membranes on the shape and cross-sectional size of aSyn fibrils

- **Findings:** The presence of model membranes has no effect on the cross-section size and shape, and  $\beta$ -strand packing in aSyn fibrils. Nor is the bilayer thickness affected.
- **Conclusions:** There is no observable incorporation of lipid molecules into the aSyn fibrils when they are formed in the presence of lipid vesicles. Furthermore, there is no impact on the area per lipid molecule in the bilayer membrane.

## Part II

- **Overarching question:** Is the formation of LBs a consequence of an organised self-assembly of aSyn fibrils and different lipid components, or is there rather a precipitation and cluster formation of insoluble fibrils that also trap different lipid components?

**Paper IV:** In this paper we investigated clusters formed by colloiddally unstable aSyn fibrils by means of small-angle neutron scattering.

- **Findings:** We observed a power-law dependence of the scattering intensity on the scattering vector,  $I \sim q^{-d}$  in all 19 samples investigated. The value of the exponent  $d = 2.6 \pm 0.3$  was independent of the sample preparation procedures and the presence of various model membrane of different concentrations.
- **Conclusions:** The arrangement of colloiddally unstable aSyn fibrils can be understood in terms of fibril clusters that have the properties of mass-fractals. The experimentally observed power law can be reproduced with a simple model of rigid-rod clusters, which can be regarded as an extension of the freely-jointed



chain (FJC) model of flexible polymers. The observed cluster arrangement can be explained by predominately attractive, mainly hydrophobic, interactions between aSyn fibrils.

**Paper V:** In this paper we investigated whether sedimenting clusters, formed of colloidally unstable aSyn fibrils at pH 5.5, are able to bind or trap lipid vesicles of various composition, with a possible connection to LB formation.

- **Findings:** Sedimentation of fibril clusters further slows down fibril fibril formation. Lipid vesicles may co-sediment together with fibrils.
- **Conclusions:** Lipids co-sediment, but it is difficult to conclude whether the co-sedimentation of lipids is due to attractive fibril-membrane interactions or whether lipid vesicles are trapped within fibril clusters.

1

# Introduction

The purpose of this chapter is to provide the reader with a rudimentary background knowledge necessary to understand most the findings presented in this thesis. The chapter begins with introduction of proteins and the forces that lead to them adopting functional, folded, forms. It also describes the way protein molecules misfold, which leads to the formation of protein aggregates, termed amyloid fibrils, that are associated with certain pathogeneses. Finally, the main players of this thesis, the protein denoted  $\alpha$ -synuclein and models of lipid cell membranes are introduced.

## 1.1 Protein folding versus amyloid fibril formation

Proteins are macromolecules that are one of the vital building blocks of living creatures. They are built from monomer units called amino acids. The sequence of amino acids residues is called primary structure and it is determined by the gene that is encoding the protein plus splicing events, if any. There are 20 genetically coded amino acids and each of them consists of a central carbon atom, known as the  $\alpha$  carbon, amino and carboxyl groups, a hydrogen atom and a side chain, or so-called R group. The R group is unique for each amino acid and it determines physical and chemical properties of the amino acid. The side chains may differ in size, shape, charge, hydrogen-bonding capacity, hydrophobic character and chemical reactivity. An illustration of an amino acid is shown in Figure 1.1 a).

When forming protein molecules, amino acids are connected end-to-end by peptide bonds. The peptide bond is formed between the carboxyl and the amino group of two amino acids by eliminating water, as illustrated in Figure 1.1 b). The remaining parts of the amino acids that are connected by the peptide bond are called amino acid residues, and they are illustrated in Figure 1.1 c)<sup>1</sup>.

A protein molecule may fold in a specific way that allows formation of hydrogen bonds between carbonyl and amine groups<sup>1</sup>. This fold is described by the so-called secondary structure. The most common forms of secondary structure are  $\alpha$ -helices and  $\beta$ -sheets. An  $\alpha$ -helix is a right-handed helix, where intramolecular hydrogen bonds are formed each 3.6 amino acid. A  $\beta$ -sheet is formed when two or more parallel or antiparallel polypeptide chains, called  $\beta$ -strands, are connected by hydrogen bonds. The distance between adjacent  $\beta$ -strands is 4.8 Å<sup>1</sup>.

The way the protein further folds in space is described by the so-called tertiary structure, and it is determined by the protein primary structure. The protein fold in three dimensions is typically a spontaneous process during which a protein assumes its native, functional structure. The process is governed by hydrophobic interactions, hydrogen bonding and van der Waals interactions<sup>2</sup>. Hydrophobic interactions lead to

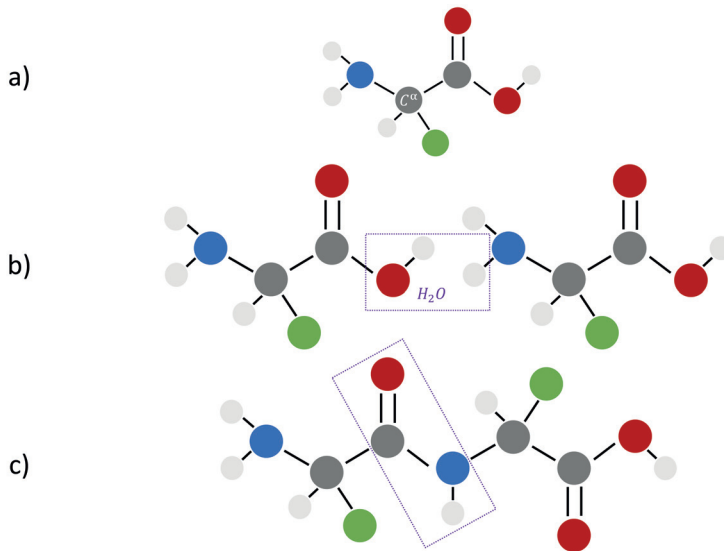


**Figure 1.1** (a) An illustration of an amino acid. The different chemical elements are shown in different colour: hydrogen in light grey, nitrogen in blue, carbon in dark grey and oxygen in red. A functional group is represented as a green circle and chemical bonds are represented as black lines. (b) The elimination of a water molecule, highlighted with purple rectangle, prior to connection of two amino acids. (c) Two amino acid residues connected by a peptide bond, highlighted with purple rectangle.

the burial of hydrophobic residues in the protein interior. Hydrogen bonds and van der Waals interactions between closely packed residues add to the protein stability by further lowering its free energy relative to the unfolded state.

It was believed, until the end of the previous century, that a protein needs to be folded so as to have a specific biological function<sup>3</sup>. However, it has been shown that not all proteins require a specific fold in order to perform their biological functions<sup>4</sup>. Such proteins are called intrinsically disordered proteins (IDPs) and suggested biological roles of IDPs are related to the process of cellular signalling and regulation<sup>3</sup>. Typically, IDPs fold upon association with a target.

The folded state of a protein is a low free energy state, with a local energy minimum. However, other structures accessible to a protein molecule have been proposed to have even lower free energy states<sup>5,6</sup>. During the folding process, the protein may go through several intermediate conformations. It is possible that these intermediates have more exposed hydrophobic surface than the final folded state. Such misfolded forms may interact with other misfolded proteins and self-assemble into well-structured protein aggregates. To ensure protein folding to the native form, molecules, such as chaperones, have a purpose to lower the energy barriers between intermedi-

ate states on the pathway to native folded state, and increase energy barriers between states that are on pathway to misfolded protein aggregates<sup>7</sup>. IDPs can also form well-structured aggregates at certain conditions in order to reduce exposure of hydrophobic groups to water. These aggregates, which can be regarded as an alternative to folded state, can have highly ordered structures.

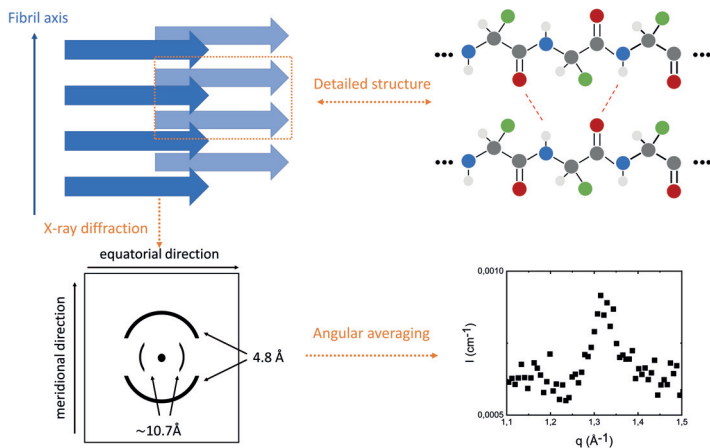


**Figure 1.2** An illustration of a cross- $\beta$  pattern and its signature on an X-ray diffraction detector. Top left: an illustration of a fibril composed of in-register parallel  $\beta$ -sheets with  $\beta$ -strands represented as blue arrows. Top right: the more detailed structure including amino acid residues of two  $\beta$ -strands. The dashed red lines are illustrating hydrogen bonds formed in between adjacent  $\beta$ -strands. Bottom left: the two reflections on a 2D detector that emerge after scattering X-rays from an aligned amyloid fibrils. Bottom right: the peak associated with the  $4.8 \text{ \AA}$  reflection obtained from angular averaging of the 2D scattering pattern.

One example of highly ordered aggregates are amyloid fibrils. Amyloid fibrils are straight, unbranched fibrils approximately  $10 \text{ nm}$  in diameter, which have a characteristic cross- $\beta$  pattern in their fibril diffraction data<sup>8</sup>. The cross- $\beta$  pattern is associated with the presence of  $\beta$ -sheets that extend parallel to the fibril axis. The pattern was first discovered by the means of X-ray diffraction when William Astbury analysed egg-whites in 1935<sup>9</sup>. The signature of the cross- $\beta$  structure at an X-ray diffraction detector are two reflections, a strong meridional reflection corresponding to the distance of  $4.8 \text{ \AA}$  between adjacent  $\beta$ -strands, and a more diffuse reflection on the equator, corresponding to an inter-sheet distance of about  $10.7 \text{ \AA}$ . In our solution wide-angle X-ray scattering (WAXS) experiments, we see the  $\beta$ -sheet repeats as a peak at  $q = 1.35 \text{ \AA}^{-1} = 2\pi/(4.8)$ . Illustrations of a fibril containing in-register parallel  $\beta$ -sheets, the reflections that are results of the X-ray scattering from amyloid fibrils, as well as angular averaged 1D scattering profile are shown in Figure 1.2. We obtained the 1D scattering profile shown in Figure 1.2 by X-ray scattering from aSyn fibrils.

## 1.2 Amyloid fibrils and disease pathogenesis

The formation of some specific amyloid fibrils and their deposition *in vivo* are hallmarks of a diverse group of diseases, referred to as amyloidoses<sup>10</sup>. These diseases are characterised by accumulation of amyloid fibrils, which often leads to progressive cell death<sup>11</sup>. The most common type of amyloidoses include neurodegenerative diseases, such as Alzheimer's disease, PD and Huntington's disease, as well as diabetes type II<sup>12</sup>. Each of these diseases is related to misfolding of specific amyloid-forming proteins.

The amyloid fibrils investigated throughout this thesis are related to PD, which is a neurodegenerative disease clinically described first in 1817 by James Parkinson<sup>13</sup>. In his essay, Parkinson described the syndrome experienced by six patients as:

*"Involuntary tremulous motion, with lessened muscular power, in parts not in action and even when supported; with a propensity to bend the trunk forwards, and to pass from a walking to a running pace: the senses and intellects being uninjured."*

PD is characterised by movement disorders such as tremor at rest, rigidity, *id est* increased resistance to passive limb movements, bradykinesia, hypokinesia and akinesia, which refer to slowness of movement, reduction in movement amplitude and absence of voluntary movement, respectively<sup>14</sup>. Apart from these movement disorder symptoms, patients diagnosed with PD also experience cognitive impairment, autonomic nervous system dysfunction, depression, sleeping disorder and decreased sense of smell<sup>15</sup>.

PD is the second most common neurodegenerative disease. Regardless of its high prevalence, it remains without cure until this day. PD is a disease of ageing and with the increases in human life spans, it is estimated that the number of people with PD will double in the period from 2005 to 2030<sup>15</sup>. The pathological hallmarks of PD are progressive loss of dopaminergic neurones in the midbrain region called *Substantia nigra pars compacta* and the presence of intraneuronal inclusions, LBs<sup>14,15</sup>. The progressive loss and dysfunction of dopaminergic neurones in the *substantia nigra pars compacta* in PD leads to the dopamine deficiency that causes the overt motor symptoms of PD<sup>16,17</sup>.

LBs are spherical inclusions that are also the hallmark of another neurodegenerative disease, called Dementia with Lewy bodies. They were first discovered in 1912 by German-American neurologist Friedrich Heinrich Lewy<sup>18</sup> and their connection with PD was found in 1919 by Tretiakoff<sup>19</sup>. LB are agglomerates that are composed of filamentous structure formed from aSyn fibrils<sup>20,21</sup>, and various cell organelles and lipid membranes<sup>22-24</sup> that seem to be trapped therein.

### 1.3 $\alpha$ -synuclein

The link between aSyn and PD was found in 1997. Firstly, the mutation in the gene coding for aSyn was associated with familial early-onset PD<sup>25</sup> and secondly, upon immunohistochemical characterisation of LBs, aSyn was found to be a major component<sup>26</sup>. In the following year, it was shown that aSyn is present in its fibrillar form in LBs, which explained the nature of the filamentous structures of the LBs<sup>20,21</sup>.

aSyn is an IDP that alternates between a natively unfolded state in the cytosol of cells and a membrane-interacting helical state<sup>27-29</sup>. It has been shown that around 15% of the total aSyn content in brain is associated with membranes<sup>30</sup>. The distinct presynaptic localization of aSyn and its interaction with highly curved membranes and synaptic proteins is indicative of a regulatory function at synapses. These potential regulatory roles include regulating synaptic activity, dopaminergic metabolism, synaptic plasticity, neurotransmitter release, learning, maintenance, or trafficking of synaptic vesicle pools<sup>31</sup>.

```
MDVFMKGLS K AKEGVVAAAE KTKQGVAAAA GKTKEGVLYV GSKTKEGVVH (50)
GVATVAEKTK EQVFNVGGAV VTGVTAVAQK TVEGAGSIAA ATGFVKKDQL (100)
GKNEEGAPQE GILEDMPVDP DNEAYEMSE EGYQDYEPEA (140)
```

**Figure 1.3** The letter coded aSyn sequence, where every letter corresponds to a single amino acid residue. Hydrophobic residues are shown in purple, the acidic residues are shown in red and the basic residues are shown in blue. The 7 amino acid repeats, responsible for the formation of  $\alpha$ -helix, are highlighted with black rectangles.

aSyn is a 140 amino acid residues long protein. The protein sequence can be divided into three parts: N-terminal, non-amyloid- $\beta$  component (NAC) and C-terminal regions. The N-terminal region, residues 1 – 60, contains several positively charged residues and is responsible for binding to lipid membranes. The NAC region, residues 61 – 95, is a hydrophobic region believed to be responsible for the formation of amyloid fibrils<sup>32</sup> and sensing of lipid properties<sup>33</sup>. The C-terminal, residues 96 – 140, is negatively charged region which is largely unstructured even when the protein is associated with lipid membranes. Throughout the N-terminal and the NAC regions, 7 amino-acid sequence repeats, containing the KTKEGV motif, are present. These repeats are responsible for the ability of aSyn to form  $\alpha$ -helices<sup>34</sup>.

## 1.4 $\alpha$ -synuclein and lipid membranes

*In vivo*,  $\alpha$ Syn interacts with cellular membranes of neurones and plasma vesicles. The membrane is a barrier that regulates trafficking of molecules from and to the intercellular environment. It is a dynamic structure, composed of lipids and proteins. Lipid molecules have diverse functions in the plasma membrane, for example, to act as a barrier, dissolve and organise membrane proteins. The function of membrane-associated proteins is to serve as transporters of various molecules across the membrane, as well as sensors between inter and intra-cellular environment. As illustrated in Figure 1.4, the lipid part of the membrane is composed of two monolayers of lipid molecules, called leaflets. This bilayer structure arises from the amphiphilic nature of the lipid molecules with the hydrophobic hydrocarbon chains being shielded from the aqueous environment, and hydrophilic head groups being exposed to it.

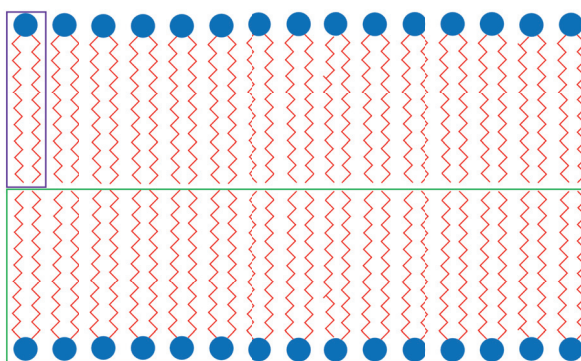


**Figure 1.4** An idealised illustration of a lipid bilayer composed of lipid molecules with two hydrophobic tails each. In reality, lipid tails are more flexible and disordered. The hydrophobic tails are shown in red and the hydrophilic head groups are shown in blue. A lipid molecule is highlighted by the purple rectangle and one bilayer leaflet is highlighted by the green rectangle.

The molecular composition of a plasma membrane can vary from cell to cell and also between the inner and outer leaflets. The most abundant lipids in the cell membrane are phospholipids, glycolipids and cholesterol. There are over 1000 different phospholipids in a mammalian cell<sup>35</sup>. Typically between 40 and 50 percent of the total amount of phospholipids in a cell membrane are the zwitterionic phosphatidylcholine (PC). Phospholipids that are more abundant in the inner leaflet of the membrane are zwitterionic phosphatidylethanolamine and negatively charged phosphatidylserine (PS)<sup>11</sup>. Other component of the outer leaflet are gangliosides<sup>36</sup>, which are a type of glycolipids, more specifically glycosphingolipids. They are mostly localised in the brain, where they comprise around 12% of total lipid amount in the neuronal membrane<sup>37</sup>.



There are many reasons for the extensive studies performed on the interaction of aSyn and lipid vesicles. *In vivo*, aSyn is expressed in the brain, which is a lipid-rich environment, and its biological function is related to trafficking of synaptic vesicles<sup>31,38</sup>. Furthermore, the presence of various lipids has been demonstrated in LBs<sup>22-24</sup> together with aSyn fibrils. It has also been suggested that interaction between aSyn and lipid membranes plays an important role in PD<sup>39</sup>.

The extensive studies of aSyn - lipid interactions have resulted in broad knowledge. It has been demonstrated that when aSyn adsorbs onto a model membrane that contain anionic lipids, it adopts an  $\alpha$ -helical structure<sup>33,40-42</sup>. Furthermore, the presence of vesicles during the fibril formation can, under certain conditions, act as an aggregation catalyser<sup>43-46</sup> and the aggregation of aSyn in the presence of a model membrane can lead to the formation of protein-lipid co-assemblies<sup>47-51</sup>. It has also been shown that oligomers have the ability to permeabilise membranes<sup>52</sup>, and that two disease related mutations, A30P and A53T may form oligomers which resemble a class of pore-forming bacterial toxins<sup>53</sup>. Pore formation in model membranes and membrane thinning due to lipid extraction upon interaction with aSyn have also been demonstrated<sup>49 54 55</sup>. Regardless of the extensive research on the subject, the role of aSyn and lipids in PD remains elusive.

# 2

# Materials

The aim of this chapter is to give insight into the sample preparation used during the experiments summarized in this thesis. It explains the protocol of aSyn expression and purification and the preparation of vesicles and fibrils.

## 2.1 $\alpha$ -synculein expression and purification

To produce aSyn, *Escherichia coli* (*E. coli*) cultures were transformed with a Pet3a plasmid containing a synthetic gene product with codons optimized for *E. coli* (purchased from Genscript, Piscataway, New Jersey). aSyn was later purified using heat treatment, ion exchange and gel-filtration chromatography. As we required pure monomers as a starting point for our experiments, we performed size-exclusion chromatography (SEC) on purified protein samples in the experimental buffer using a 24 mL Superdex75 column (GE healthcare).

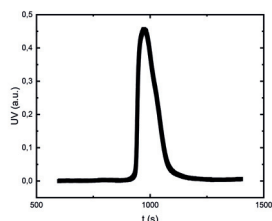


**Figure 2.1** Dependence of UV absorbance on time. The monomers are eluting ca. 1000 s after the injection of the protein solution into the column.

SEC is a technique used to separate particles by their size. A usual SEC instrument contains a column filled with porous beads, a pump and an absorbance ultraviolet (UV) detector. The beads in the column contain pores different sizes. As the solution containing particles of different sizes is pumped through the column, the largest particles are the first to be eluted, as they will only be accommodated in the largest pores. In order to obtain protein monomers, fractions eluting at volumes of interest were collected. The protein concentration was measured using the integrated absorbance at 280 nm of the collected fraction from the SEC chromatogram and the molar extinction coefficient  $5800 \text{ M}^{-1} \text{ cm}^{-1}$ . The UV absorbance spectrum at the time of monomer elution (ca. 1000 s) is shown in Figure 2.1. In order to obtain the high protein concentration necessary for certain experiments, monomers collected from SEC were lyophilised and resuspended in a smaller volume.

Deuterated aSyn was used in some experiments. An *E. coli* cell pellet containing deuterated aSyn was prepared at the Deuteration Laboratory of the Institute Laue Langevin (ILL) in Grenoble, France and purified as described in<sup>40</sup>. The degree of deuteration was 75%, as determined using mass spectrometry. Deuterated aSyn monomers were isolated utilising SEC technique, as described above.

## 2.2 Model membrane preparation

The model membranes used in experiments included in this thesis were produced by either extrusion or sonication. Prior to each preparation procedures, the lipid powder was weighed and a defined ratio of two lipids was dissolved in a chloroform/methanol solvent, due to high solubility of lipids in organic solvents. After dissolution, the solvent was evaporated underneath a stream of N<sub>2</sub> gas, leaving a lipid film. The film was further dried in a vacuum oven over night. The dry lipid film was dispersed in a buffer resulting in the formation of large and often multilamellar vesicles. Through the input of mechanical energy, these vesicles can be fragmented into smaller unilamellar vesicles (SUVs) and/or lipid disc micelles. Two common fragmentation methods are extrusion and sonication.

The model membranes used in this thesis were lipid vesicles and lipid disc micelles, composed of various mixtures of two lipids. Most of the time, the two lipids used were phospholipids, PC and PS, but sometimes PC was used in combination with gangliosides. The PCs used were 1,2-dimyristoyl-sn-glycero-3-phosphocholine (DMPC), 1-palmitoyl-2-oleoyl-glycero-3-phosphocholine (POPC) and 1,2-dioleoyl-sn-glycero-3-phosphocholine (DOPC). The PS used were 1,2-dimyristoyl-sn-glycero-3-phospho-L-serine (DMPS), 1-palmitoyl-2-oleoyl-sn-glycero-3-phospho-L-serine (POPS) and 1,2-dioleoyl-sn-glycero-3-phospho-L-serine (DOPS) and the gangliosides used are GM1 and GM3. The chemical structures of the lipids used throughout this thesis are summarised in Figure 2.2.

## 2.3 Fibril formation

*Fibrils were stirred, not shaken.*

Fibrils were formed from aSyn monomers collected from SEC and incubated at 37° C in a pure buffer solution or in a vesicle dispersion. As fibril formation is a pH dependent process<sup>56</sup>, and is significantly slower at pH higher than 5.5, when working at high pH we accelerated the fibril formation process by agitation during the incubation. The mechanical agitation, which we are inducing by stirring with a magnetic bar, accelerates the fibril formation by increasing elongation rate due to increased fibril fragmentation<sup>57</sup>.

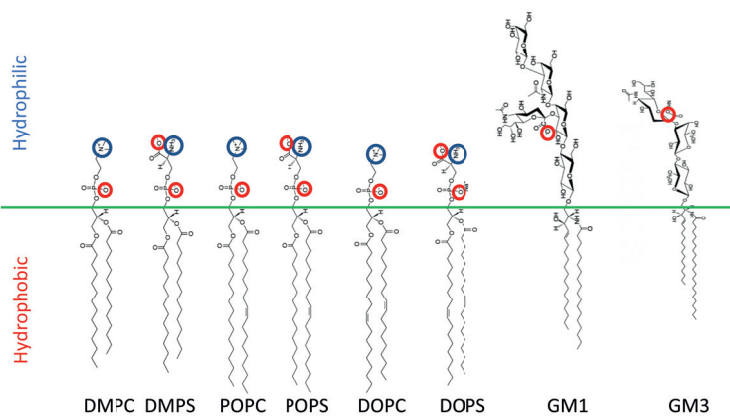


**Figure 2.2** The chemical structures of lipid molecules investigated throughout this thesis. The green line marks the border between the hydrophilic head groups and the hydrophobic tails of the lipid molecules. Positively and negatively charged parts of the molecules are indicated by red and blue circles, respectively.

# 3

# Methods

In this chapter, the experimental techniques used in the experiments presented throughout this thesis are introduced.

### 3.1 Scattering

In scattering techniques, a sample of interest is irradiated with an incident radiation. When the incident radiation is passing through the sample, most of it is transmitted, whereas the rest can either be absorbed or scattered. In scattering techniques, one analyses the amount of the scattered radiation and the angles that the radiation is scattered at. Scattering techniques are widely used for the investigation of objects ranging from 1 nanometre to 20 micrometres. These techniques found applications in various disciplines, including physics, chemistry, biology, engineering and material sciences. They can provide information about particle size, shape and structure, as well as about interactions between particles in solution. Scattering methods are complementary to imaging, with one advantage being that the structures can be examined directly in solution.

The scattering techniques are divided according to the type of the incident radiation to light, neutron or X-ray scattering. The most intuitive form of scattering, that of the visible light, occurs when there are variations in a refractive index in the medium illuminated by the visible light. Scattering of neutrons happens due to interaction of neutrons and atomic nuclei, whereas the scattering of X-rays occurs due to interaction of X-rays and electrons in atomic orbitals.

A scattering event is characterised by changes in momentum and energy of the incident radiation. When the energy is conserved, the process is known as elastic scattering, otherwise, the process is referred to as inelastic scattering. Throughout this book, I will be talking about elastic scattering.

Incident radiation, which can be regarded as an electromagnetic wave, is described by a wave vector defined as

$$\vec{k}_i = \frac{2\pi}{\lambda} \vec{e}_i, \quad (3.1)$$

where  $\lambda$  is the wavelength of the radiation propagating in the direction  $\vec{e}_i$ . After an elastic scattering event, the wave vector changes the direction of propagation but its magnitude remains constant. The wave vector of the scattered wave we denote  $\vec{k}_s$ . Figure 3.1 shows an illustration of a scattering experiment.

It is common in practice to use a momentum transfer rather than the scattering angle,  $\theta$ , to describe scattering event. The momentum transfer,  $q$ , or the scattering vector is

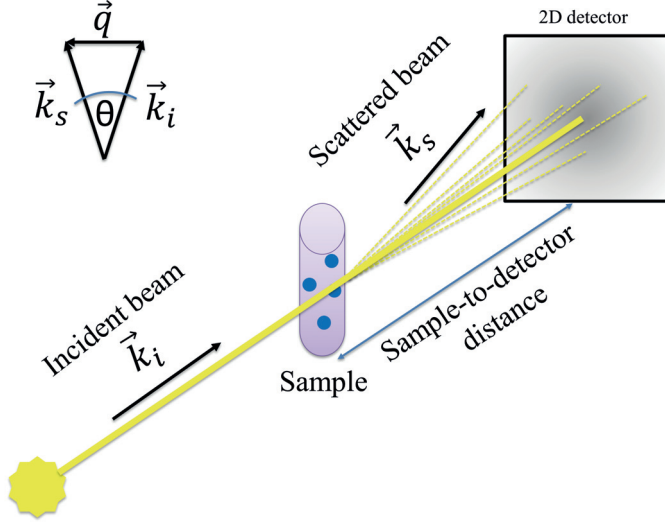


**Figure 3.1** A schematic illustration of a scattering experiment. A part of an incident beam, with the wave vector  $\vec{k}_i$ , is being scattered after interacting with a sample. The scattered radiation with the wave vector,  $\vec{k}_s$ , is detected by a 2D detector. In the top left illustrated is scattering at angle  $\theta$  and the  $\vec{q}$  vector, defined as the difference between  $\vec{k}_s$  and  $\vec{k}_i$ .

defined as

$$\vec{q} = \vec{k}_s - \vec{k}_i. \quad (3.2)$$

As can be concluded from a diagram shown in top left corner of Figure 3.1, the magnitude of the scattering vector is

$$q = \frac{4\pi}{\lambda} \sin \frac{\theta}{2}. \quad (3.3)$$

That the scattering vector includes information about both radiation wavelength and the scattering angle justifies its utilisation in the practice. The quantities given as a function of  $\vec{q}$  are in reciprocal space and quantities expressed as a function of  $\vec{r}$  are in real space. The relation between reciprocal and real space,  $q = 2\pi/d$ , is an intuitive way of deducing the length scales,  $d$ , accessible at certain  $q$  values.

In the case of elastic scattering, the amplitude,  $\Psi$ , of the wave scattered from an assembly of  $N$  atoms is given by<sup>58</sup>:

$$\Psi(\vec{q}) = \sum_{i=1}^N b_i e^{-i\vec{q} \cdot \vec{r}_i}, \quad (3.4)$$

where  $\vec{r}_i$  is the coordinate of the  $i^{th}$  atom and  $e^{-i\vec{q} \cdot \vec{r}_i}$  is the phase factor which is a consequence of interference of waves scattered by different  $N$  atoms.  $b_i$  is the scattering



length, which measures how strongly an atom interacts with the incident radiation. In the case of X-rays, the scattering length depends on the number of electrons in the atom and it is, therefore, increasing with atomic number. In the case of neutrons, the scattering length is varying randomly through the periodic table of elements and is a consequence of the interaction between a neutron and the atomic nuclei.

Measured in a scattering experiment is the intensity distribution of scattered radiation as a function of scattering angle, which is related with the amplitude of the scattering wave by:

$$I = |\Psi(\vec{q})|^2 = \Psi(\vec{q})\Psi^*(\vec{q}), \quad (3.5)$$

where  $\Psi^*(\vec{q})$  denotes the complex conjugate of the scattering amplitude ( $\Psi^*(\vec{q}) = \sum_{i=1}^N b_i e^{i\vec{q}\cdot\vec{r}_i}$ ). As the exponential terms cancel out, it is obvious that the complex conjugation results in loss of information on the phase of the scattered wave. This issue is known as “the phase problem” the consequence of which is that we cannot do an inverse Fourier transformation and that *a priori* knowledge of the sample is necessary in order to deduce the structure of the scattering objects.

### 3.1.1 Static Scattering

In static scattering, the measured scattering intensity is averaged over time. From the static scattering one gets information about shape and size of particles, their internal structure and interaction between particles.

The quantity that describes a probability that the incident radiation will be scattered when passing through the medium is the so-called scattering cross-section,  $\sigma$ . It is defined as the number of scattered particles normalised by the incident flux. The normalisation is performed to ensure that the quantity is an intrinsic property, independent on the incident flux. In the case of the coherent scattering, where waves scattered from different part of a sample interfere with each other, the scattering cross-section is given by<sup>59</sup>

$$\sigma = 4\pi|b|^2. \quad (3.6)$$

The form of the cross section we are after in the scattering experiment is the volume specific differential scattering cross section

$$\frac{d\Sigma}{d\Omega} = n \frac{d\sigma}{d\Omega}, \quad (3.7)$$

where  $n$  is the particle density and  $\Omega$  is a solid angle. The volume specific differential cross section has unit of inverse length, and it contains information about size,

shape, internal structure of scattering particles and inter-particle interactions. It is also known as the absolute scattering intensity. It does not depend on the experimental setup, such as the particle flux, size of the beam, detector efficiency, nor on the sample volume. It only depends on the properties of the sample.

The absolute intensity can be expressed as:

$$\frac{d\Sigma(q)}{d\Omega} = \phi V_p \Delta\rho^2 P(q) S(q), \quad (3.8)$$

where  $\phi$  is the particle volume fraction,  $V_p$  is the particle volume,  $\Delta\rho$  is the contrast factor,  $P(q)$  is the particle form factor and  $S(q)$  is the structure factor.

The contrast factor,  $\rho = \sum_i b_i / V_p$ , where the sum is over all atoms in the molecule or particle (assembly of molecules), is the total scattering length divided by the particle volume, termed scattering length density (SLD). The contrast factor from equation 3.8,  $\Delta\rho$  is defined as a difference of particle and solvent SLDs.

The form factor,  $P(q)$ , provides an information about structure and size of scattering particles. It is given by a Fourier transform of the SLD difference

$$P(q) = \int_{V_p} \Delta\rho(q) e^{-iqr\cos\delta} dr, \quad (3.9)$$

where integration is performed over the entire particle volume,  $V_p$  and  $\delta$  is an angle between  $\vec{q}$  and  $\vec{r}$ .

The last term in equation 3.8 is the structure factor. It provides information about the relative positions of particles and hence on the interactions between particles. It can be expressed as a Fourier transform of the radial distribution function,  $g(r)$ , which for spherical particles can be written as

$$S(q) = 1 + 4\pi \frac{N_p}{V} \int_0^\infty (g(r) - 1) r^2 \frac{\sin(qr)}{qr} dr, \quad (3.10)$$

where  $N_p$  is the number of particles and  $V$  is the total volume of the sample. The radial distribution function gives the probability of finding the centre of another particle at a distance  $r$  from an arbitrarily selected particle<sup>59</sup>.

### 3.1.2 Data modelling

Modelling of scattering data normally implies testing different model structures, such as spheres, cylinders, shells (vesicles), etc, and finding the model parameters that best agree with the experimental data.

One such model is the Debye model, which is a good approximation of the scattering of a flexible polymer coil in solution<sup>60</sup>. The Debye form factor is given by

$$P(q) = 2(e^{-qR_g} + qR_g - 1)/(qR_g)^2, \quad (3.11)$$

where  $R_g$  is the radius of gyration of the polymer. The Debye function is a good approximation of the scattering of monomeric aSyn. In Figure 3.2a shown is the Debye function with  $R_g = 4$  nm, which corresponds to the radius of gyration of aSyn monomer.

In the limit of  $q \leq 1/R_g$ , scattering intensity can be approximated as<sup>59</sup>:

$$I(q) = I_0 e^{-(q^2 R_g^2)/3}. \quad (3.12)$$

The equation 3.12 is known as the Guinier equation and it provides an estimate of the radius of gyration by applying an exponential fit to the data in the low- $q$  regime.

Modelling data in the so-called Porod region, *id est*  $q \gg 1/r$ , where  $r$  is the size of a scattering object, yields information on structural dimensionality, which is the fractal dimension of the scattering object, usually referred to as  $d$ .

The combination of Guiner and Porod models, known as the Unified Exponential/Power-law or Beaucage model, was derived by Gregory Beaucage in 1995<sup>61</sup> and corrected in 1996<sup>62</sup>. The Beaucage model is useful for modelling mass fractals, which are fractal objects with  $5/3 \leq d \leq 3$ . The scattering intensity, in such case, can be expressed as

$$I(q) = G e^{-(q^2 R_g^2)/3} + \frac{C}{q^d} \left( \text{erf} \left( \frac{q R_g}{6^{1/2}} \right) \right)^{3d}, \quad (3.13)$$

where  $G$  is the Guinier scaling factor,  $C = \frac{Gd}{R_g^d} \left( \frac{6d^2}{(2+d)(2+2d)} \right)^{d/2} \Gamma(\frac{d}{2})$  is the Porod scaling factor with  $\Gamma(\frac{d}{2})$  being the gamma function, and  $\text{erf}(\frac{qR_g}{6^{1/2}})$  is an error function which provides smooth transitions between Guinier and Porod regions<sup>63</sup>. In this thesis, the Beaucage model has been found useful when fitting modelled fibril clusters that were used to analyse experimentally observed arrangement of aSyn fibrils, as discussed in 3.1.3. In Figure 3.2b, shown is the Beaucage model for  $G = 1.6 \times 10^9$ ,  $d = 2.3$  and  $R_g = 300$  nm.

For various shapes, such as cylinders, elliptical cylinders, core-shell cylinders, lamellar object, etc. one can find calculated analytical models of form factors. One then compares scattering data with analytical form factors for various parameters included in the analytical expressions. By finding the parameters that best agree with the data,

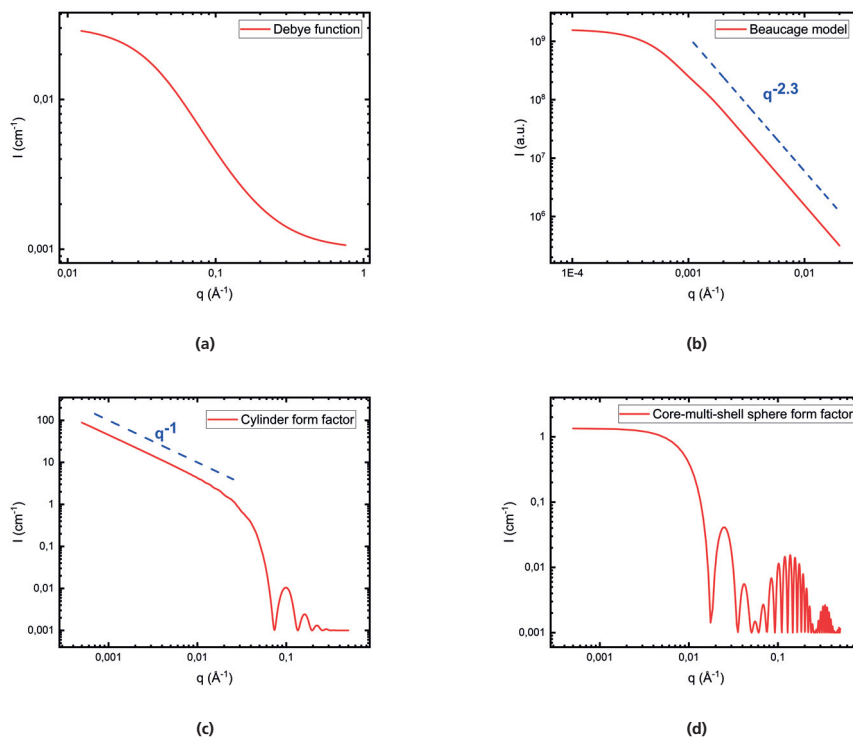


**Figure 3.2** a) The Debye function with  $R_g = 4$  nm represented with solid red line. b) The Beaucage model with  $G = 1.6 \times 10^{-9}$ ,  $R_g = 300$  nm and  $d = 2.3$  represented with solid red line. The dashed blue line represents the power law dependence of the scattering profile, with a power value equal to 2.3. c) The analytical form of a cylinder form factor with the radius of 5.2 nm and the cylinder length of 4000 nm, corresponding to aSyn fibril dimensions, represented with solid red line. The dashed blue line represents the power law dependence of the scattering profile, with a power value equal to 1. d) The analytical form factor of core-multi-shell model particles composed of three shells, modelling the scattering response of e.g. spherical bilayer vesicles.

one learns about the sample properties. Analytical expressions for the form factor models derived for various shapes can be found in<sup>60</sup>.

A form factor contains the complete information of the size and shape of the particle. When samples are dilute, so that the interactions can be neglected, the structure factor,  $S(q)$ , in Equation 3.8 is equal to one, and one can obtain the experimental form factor from the absolute intensity.

Some of the form factor models used throughout this thesis were that of a cylinder and a core-multi-shell sphere. The cylinder form factor, with a cross-sectional radius of 5.2 nm was used to model the scattering of aSyn fibrils. The core-multi-shell form factor, with 3 shells, was used to model the bilayer scattering, where the innermost

and the outermost shells represent the inner and the outer head group layers, and the middle shell represents the acyl chain layer.

The analytical expression for the form factor of a cylinder with radius  $R$  and length  $L$  is given by<sup>60</sup>

$$P_c(q) = \int_0^{\pi/2} \left( \frac{2J_1(qR\sin\alpha)}{qR\sin\alpha} \frac{\sin(qL\cos\alpha)/2}{(qL\cos\alpha)/2} \right)^2 \sin\alpha d\alpha, \quad (3.14)$$

where  $J_1(x)$  is the first order Bessel function. A signature of the long cylinder form factor for  $q > 1/R_g$  is a power law dependence of the scattering intensity on the  $q$ -vector, with a power equal to  $-1$ ,  $I \sim q^{-1}$ .

The form factor of a core-shell sphere with 3 shells, is given by<sup>60</sup>

$$P_v(q) = \frac{I}{M} \left( \rho_1 V(R_1) F(I, R_1) + \sum_{i=2}^4 (\rho_i - \rho_{i-1}) V(R_i) F(q, R_i) \right)^2 \quad (3.15)$$

where  $F(q, R_i) = 3(\sin(q, R_i) - qR_i\cos(q, R_i))/qR_i^3$  is the form factor amplitude of a sphere with radius  $R_i$ ,  $M = \rho_1 V(R_1) + \sum_{i=2}^3 V(R_i)(\rho_i - \rho_{i-1})$  is the total scattering length of the core-shell particle,  $V(R_i) = 4\pi R_i^3/3$  is the volume of the sphere with radius  $R_i$ , and  $\rho_i$  is the scattering length density of the  $i$ -th shell<sup>60</sup>.

Figure 3.2 shows the cylinder and the core-multi-shell sphere form factors calculated using the analytical equations 3.14 and 3.15, respectively. The form factor parameters correspond to the ones used to describe the experimental data in Paper III, excluding the polydispersity. The polydispersity is included in the modelling of the scattering data to account for a co-existence of particles with different size and shape, which often occurs in practice.

### 3.1.3 Modelling of fibril clusters and the Debye scattering equation

In this work we have developed a method to model the scattering of fibril clusters. In our model of fibril clusters, individual fibrils were modelled as infinitesimally thin rods, represented by straight strings of 100 distinct monomers, regarded as point scatterers, separated by a distance of 1 nm. The clusters were constructed by stepwise addition of fibrils of random orientation. The fibrils were connected with each other, with fibril  $\#N$  connected to fibril  $\#(N-1)$  and fibril  $\#(N+1)$ .

The developed method includes the possibility to tune the density of the modelled clusters by alternating the way that fibrils within the clusters are connected. The

most dense clusters were created by connecting each fibril to the previous one at the monomer #50, *id est*, at the position of the middle monomer. The cluster with lowest density were created when fibrils were connected end-to-end. The cluster having density in between the limits were created by each fibril being connected to the previous one at randomly chosen connection points. An example of such cluster (fibrils connected at randomly chosen positions) is shown in Figure 3.3.

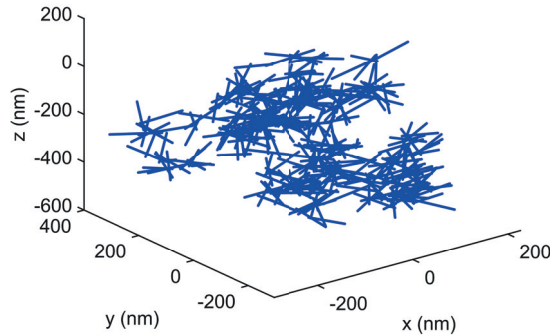


**Figure 3.3** An example of a modelled fibril cluster with 400 fibrils, each containing 100 monomers at a 1 nm separation. Fibrils are connected at randomly chosen positions.

The scattering intensity of the modelled cluster was calculated by employing the Debye scattering equation (DSE)<sup>64</sup>. DSE is used for the calculation of scattering intensity from isotropic samples and the intensity calculated by DSE is spherically averaged. If we assume that the adsorption of incident radiation is negligible, the scattering length is a real number and  $b^* = b$ . The scattering intensity, given by equation 3.5, becomes

$$I = \sum_{i=1}^N \sum_{j=1}^N b_i b_j e^{-i\vec{q} \cdot (\vec{r}_i - \vec{r}_j)} = \sum_{i=1}^N \sum_{j=1}^N b_i b_j e^{-iqr_{ij} \cos(\theta)}, \quad (3.16)$$

where  $\theta$  is the angle between  $\vec{q}$  and  $\vec{r}_i - \vec{r}_j = r_{ij}$ . Spherical averaging of the equation 3.16 gives

$$I = \sum_{i=1}^N \sum_{j=1}^N b_i b_j \frac{\sin(qr_{ij})}{qr_{ij}}. \quad (3.17)$$

Equation 3.17 is the DSE.

### 3.1.4 Contrast matching neutron scattering

Neutrons interact with the atomic nuclei via strong nuclear interactions. The interaction, *id est*, the neutron scattering length, depends on the properties of the nuclei. As the properties of the hydrogen nucleus and the nucleus of its isotope deuterium differ due to the presence of a neutron in the latter, there is a big difference in scattering lengths of hydrogen ( $b_H = -3.739$  fm) and deuterium ( $b_D = 6.67$  fm).

This difference is utilised in a technique known as contrast matching. Contrast matching is a convenient technique when the system investigated is composed of two or more distinct particles. By varying the ratio of H<sub>2</sub>O and D<sub>2</sub>O in the solvent, one can match the SLD of the solvent to the SLD of one of the particles. The analysis of the scattering pattern provides information about the particle that has the SLD different from that of the solvent, whereas there is no scattering which is a consequence of interaction between neutrons and the matchout particle.

The bi-component systems studied throughout this thesis are composed of protein and lipid membranes. To more easily extract useful information about the system from scattering experiments, contrast matching experiments were performed. Using partially deuterated proteins (degree of deuteration 75%) and protonated lipids suspended in D<sub>2</sub>O buffer, the SLDs of the solvent and the protein were matched and the observed scattering was solely due to the interaction between neutrons and the lipid molecules. These experiments provide information about the morphology of the lipid components in the system. In Figure 3.4, an illustration of contrast matching when the sample is composed of protein and lipid vesicles is shown. The middle part of the Figure illustrates the previously mentioned contrast matching experiments discussed in this thesis and Papers I and II.

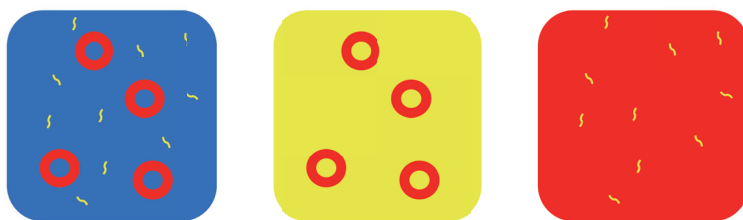


**Figure 3.4** An example of contrast matching where the difference in colour symbolises a difference in SLD. Left: protein (yellow) and vesicles (red) are suspended in a solvent (blue) not matching any of the particles. Middle: contrast matching of the protein molecules using a solvent with the same SLD as protein (yellow). Right: contrast matching of the lipid vesicles by using a solvent with the same SLD as lipid (red).

### 3.1.5 Dynamic light scattering

In dynamic scattering experiments, one uses coherent incident radiation. For that reason, in dynamic light scattering (DLS) methods one typically uses a laser beam as its incident radiation. As particles in solution change their position due to Brownian motion, the phase of the scattered waves is also changed. The resulting interference of the scattered waves provides a specific pattern at the detector, a so-called “speckle” pattern. These random fluctuations of the scattered intensity can be used to determine the diffusion coefficient of the particles in the solution, which at low enough concentrations provides information about the effective size of the particles.

The outcome of a DLS experiment is the intensity correlation function, which compares the intensity at time zero to the one after a delay time  $\tau$ , at the same detector point. The intensity correlation function is defined as<sup>59</sup>

$$g^2(\vec{q}, t) = \frac{\langle I(\vec{q}, 0)I(\vec{q}, \tau) \rangle}{\langle I(q) \rangle^2}. \quad (3.18)$$

The quantity of interest in a DLS experiment is a so-called field correlation function,  $g^1(\vec{q}, \tau)$ . It is related to the intensity correlation function via the Siegert relation<sup>59</sup>

$$g^2(\vec{q}, \tau) = 1 + \beta g^1(\vec{q}, \tau)^2, \quad (3.19)$$

where  $\beta$  is an instrument constant. In turn,  $g^1(\vec{q}, \tau)$  is related to the diffusion coefficient  $D$  through<sup>59</sup>

$$g^1(\vec{q}, \tau) = e^{-Dq^2\tau}. \quad (3.20)$$

At high enough dilution, where interparticle interactions can be neglected, the diffusion coefficient is related to the hydrodynamic radius,  $R_H$ , of the particles via the Stokes-Einstein equation

$$D = \frac{k_B T}{6\pi\eta R_H}, \quad (3.21)$$

where  $k_B = 1.38 \times 10^{-23} \text{JK}^{-1}$  is the Boltzmann constant,  $T$  is the temperature and  $\eta$  is the solvent viscosity.

DLS invokes  $q \approx 10^{-1} \text{\AA}^{-1}$  and hence collective dynamics on length scale of 100 nm

## 3.2 Nuclear magnetic resonance

Nuclear magnetic resonance (NMR) is a powerful spectroscopic technique that utilises radio frequency irradiation. NMR spectroscopy detects signals from individual nuclei



that posses a non-zero spin and, hence, a magnetic moment. The technique provides information about the atomic composition of molecules, chemical environment of a each nucleus and how nuclei are related to each other in space.

In a typical NMR experiment, a sample is placed in a strong magnetic field,  $\vec{B}_0$ . This results in non-zero magnetization of the sample, caused by preferred alignment of the nuclei magnetic moments in the direction of the magnetic field. By convention, the direction of the magnetic field is along the  $z$ -axis of a laboratory coordinate system. The magnetic field exerts a torque onto the nuclei magnetic moments, making them precess around the magnetic field direction. The frequency of precession is called the Larmor frequency  $\omega$ , equal to  $\omega = -\gamma B_0$ , where  $\gamma$  is the gyromagnetic ratio and  $B_0$  is the magnitude of the external magnetic field<sup>65</sup>. A short radio-frequency (RF) pulse, with a frequency near the Larmor frequency, is applied perpendicular to the  $\vec{B}_0$  direction. The applied RF pulse flips the nuclei magnetic moments, resulting in the emergence of a component of the magnetization vector in the  $x - y$  plane. This precessing magnetization vector in the  $x - y$  plane induces a current which is what is recorded as a time domain signal called the free induction decay (FID).

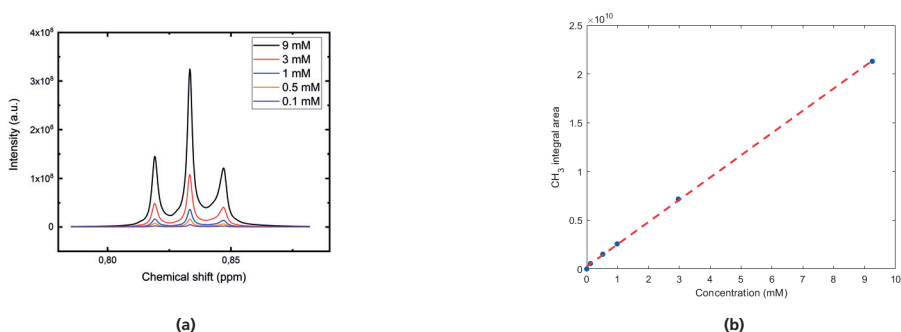


**Figure 3.5** (a)  $CH_3$  decane peaks used for the construction of a calibration curve. (b) The calibration curve.

Being a spectroscopy technique where energy is adsorbed from the RF radiation, the signal intensity (adsorbed amount) is proportional to the concentration. NMR was used in this thesis to quantify the lipid concentration of the samples. In order to determine concentration by means of NMR, one needs to calibrate against a known standard. The standard can be either internal or external. Using an internal standard involves addition of a known amount of a certain substance to the samples whose concentration one wants to determine. An external standard of a known concentration is used for construction of a calibration curve that is further used for the concentration determination. In this thesis, a decane solution in a mixture of deuterated chloroform and deuterated methanol (standing in 3/1 volume ratio) was used as an external standard. In Figure 3.5a the  $CH_3$  peaks coming from a decane solutions at 5

different concentrations are shown. The calibration curve, shown in Figure 3.5b, was constructed by integrated the areas of all 5  $CH_3$  peaks.

### 3.3 Cryogenic transmission electron microscopy

Cryogenic transmission electron microscopy (cryo - TEM) is an imaging technique that allows nanometre resolution. This high resolution is possible due to the use of an electron beam, with wavelengths smaller than a nanometre, rather than the visible light, which allows resolution of only a couple of hundreds of nanometres.

In TEM, the sample is illuminated by the electron stream, and the transmitted electrons are focused by a magnetic lens onto a detector<sup>66</sup>. The specific feature of the cryo - TEM technique is that it provides us with a snapshot of a dynamic system. This is achieved by freezing the sample to cryogenic temperatures, usually lower than 140 K. This freezing at low temperature is sufficiently fast to prevent formation of ice crystals<sup>67</sup>.

### 3.4 Circular dichroism spectroscopy

Circular dichroism (CD) is a spectroscopic technique used for investigation of the protein secondary and tertiary structure. It is a type of adsorption spectroscopy where a sample is illuminated by a circularly polarised light, right or left polarisations. In CD spectroscopy, the difference in adsorption of the left and the right polarised components is measured<sup>68</sup>. In order to have a difference in the adsorption of the left and the right polarisation, the sample must contain chiral-molecules, *id est*, molecules whose mirror image is not identical to the molecule itself. Amino acids are one example of the chiral molecules.

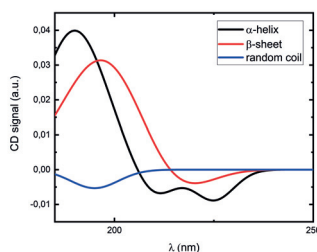


**Figure 3.6** An illustration of CD spectra when protein has  $\alpha$ -helica (black),  $\beta$ -sheet (red) and random coil (blue) conformation.

The CD signal in a far-UV range (250 – 185 nm) depends on the protein secondary structure and specific secondary structure motifs have different signals. Figure 3.6

shows an illustration of the CD signals coming from proteins if having an  $\alpha$ -helical,  $\beta$ -sheet or a random coil structure.

When adsorbed onto a lipid membrane, aSyn adopts an  $\alpha$ -helical conformation and CD spectra were therefore used as an indicator of aSyn adsorption onto lipid membranes.

# 4

## $\alpha$ -synuclein: amyloid fibrils and interactions with lipid membranes

*"The cleverest of all, in my opinion, is the man who calls himself a fool at least once a month."*

*-Fyodor Mikhailovich Dostoevsky*

In this chapter we are discussing the results summarised in the 5 papers included in this thesis. The discussion can be divided in 2 parts. In section 4.1 we are looking at interaction between model lipid membranes and aSyn. We are investigating the monomer adsorption onto model lipid membranes and the fibril formation in the presence of lipid membranes. We study these interactions in simplified systems in order to gain insight into the nature of both the biological function of aSyn and a possible mechanism of cell death in PD, that is proposed to be membrane disruption during aSyn fibril formation (Paper I and II). We are also discussing the possible co-assembly formation when the fibrils are being formed in the presence of membranes (Paper III). Section 4.2 contains analyses of aSyn fibril arrangements that resemble the ones found in LBs, which are also included in Papers IV and V.

Before starting a discussion of the results, I would like to bring to the reader's attention that different solution conditions were used in different experiments. The solution conditions, such as pH, are important due to the polarised charge distribution of aSyn molecules, which has the consequence that aSyn behaves differently when the solution pH is altered. For example, the process of aSyn aggregation at  $\text{pH} < 6$  is dominated by secondary nucleation, whereas at  $\text{pH} > 6$  the fibril formation process is dominated by elongation<sup>56,70</sup>. At  $\text{pH} 5.5$ , aSyn fibrils aggregate further into dense, sedimenting, clusters, whereas at  $\text{pH} 6$  and higher, aSyn fibrils form a sample-spanning network<sup>71</sup>. The interaction with lipids has also been shown to be pH dependent<sup>44,46,72,73</sup>. For example, the presence of vesicles containing gangliosides has been shown to accelerate fibril formation at  $\text{pH} 5.5$ <sup>46</sup> and to inhibit it at  $7.5$ <sup>73</sup>. In Papers I, IV and V experiments were performed at  $\text{pH} 5.5$ , whereas in Papers II and III experiments were performed at  $\text{pH} 6.0, 6.5, 7.0$  and  $7.4$ .

## 4.1 Part I: aSyn–membrane interactions and co-assembly formation

Despite more than 30 years of research, the normal physiological functions of  $\alpha$ -synuclein remain obscure. However, some of the suggested roles are listed as follows. It has been reported that at the presynaptic terminal aSyn interacts with numerous proteins such as: Rab3, Synaptobrevin-2, Synapsin III, Vesicular-monoamine transporter 2 (VMAT2) and tyrosine hydroxylase<sup>74,75</sup>. Interactions with these proteins are strongly suggesting a role at synapses. aSyn can induce membrane curvature<sup>76,77</sup>, bind fatty acids<sup>78</sup>, and bears similarities with class A2 apolipoproteins, which suggests a role in lipid metabolism. It has also been reported to influence phospholipid composition<sup>79</sup> and organise membrane components<sup>80</sup>. aSyn has further been demonstrated to bind and regulate the activity of the dopamine transporter DAT<sup>81</sup> and to

decrease dopamine synthesis<sup>74,75</sup>. These findings taken together could suggest that the dopaminergic system has a higher need for aSyn but also an increased susceptibility to aSyn dysfunction. In pre-synaptic terminals aSyn facilitates the formation of the soluble N-ethylmaleimidesensitive factor attachment protein receptor (SNARE) complex, a protein complex that mediates membrane fusion between synaptic vesicles and the synaptic terminal membrane<sup>38</sup>. The fusion of synaptic vesicles at the membrane leads to neurotransmitter release into the synaptic cleft, meaning that aSyn might be essential for normal neuronal signalling.

The formation of co-assemblies containing aSyn and lipids has been previously observed in numerous studies where it has been established that lipids present during the fibril formation may be taken up in the fibrillar aggregates<sup>47-51</sup>. However, it is still not known at which stage of the process the co-aggregates are forming, what is the location of lipids in those co-aggregates and whether the association of lipids and fibrils is internal, with lipids being incorporated in the fibril structure on a molecular lever, or external, where bilayers or monolayers are adsorbed onto the fibril surface.

It has been proposed that the basis of the cell death in amyloidosis is a disruption of cell membranes through interactions between amyloid proteins and membrane lipids<sup>11,39,82,83</sup>. The membrane disruption and dysfunction of cell organelles, in particular mitochondria<sup>84</sup>, lysosomes<sup>85</sup> and Golgi apparatus<sup>86</sup>, have been reported in PD patients. Experiments both *in vivo*<sup>87,88</sup> and *in vitro*<sup>89,90</sup> demonstrated the disruption of neuronal cell membranes as a consequence of interaction with aSyn oligomers. There have also been numerous experiments that looked into disruption of model membranes upon interaction with aSyn<sup>47-49,54,55</sup>. Different mechanisms of membrane disruption have been proposed. One of the proposed mechanisms is the pore formation and membrane thinning due to lipid extraction<sup>49,54,55</sup>.

#### **4.1.1 POPC/POPS vesicles with adsorbed aSyn are stable structures and the adsorbed amount depends on the membrane charge**

As it has been suggested that the biological function of aSyn involves interaction of aSyn monomers and synaptic vesicles, we investigated the adsorption of monomeric aSyn onto lipid vesicles. The vesicles were composed of the combination of two unsaturated phospholipids, POPC and POPS. Interaction of monomeric aSyn and model lipid membranes was investigated by means of CD spectroscopy, DLS and small-angle X-ray scattering (SAXS). The experiments were performed using samples in 20 mM phosphate buffer at pH 7.0. The results discussed in this section are also presented in Paper II.

When aSyn monomers are added to a vesicle dispersion, adsorption is immediate.

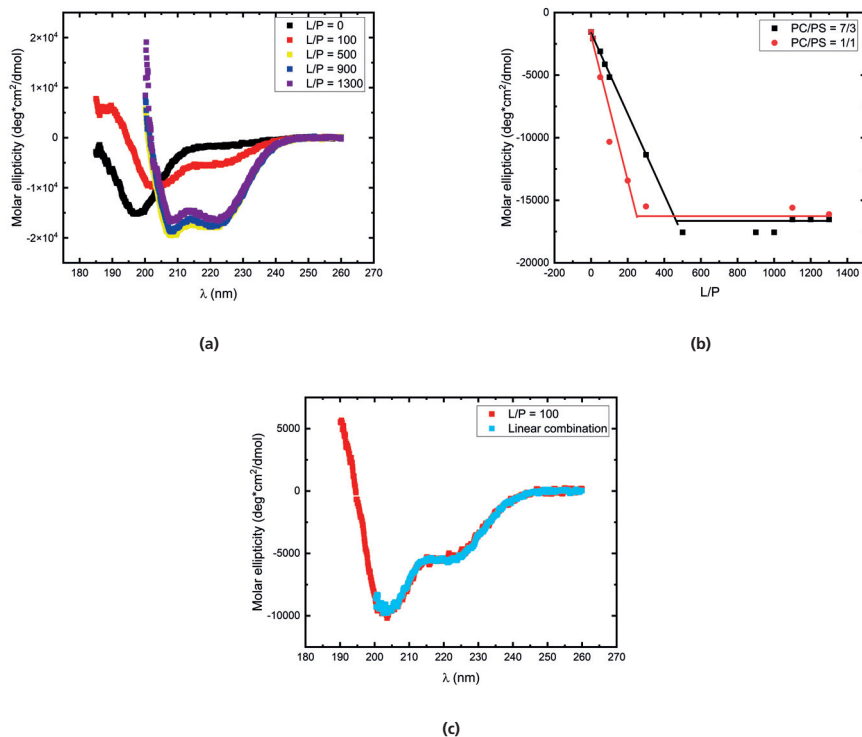


**Figure 4.1** (a) CD pattern for different L/P ratios when vesicles are composed of 30% PS at aSyn concentration of 7  $\mu$ M. (b) Value of the CD signal at 222 nm vs. L/P ratio when vesicles were composed of 30% (black) and 50% (red) PS. (c) Comparison between CD profile for L/P=100 (red squares) and linear combination,  $CD_{LC}$  (blue squares) of CD profiles at L/P = 0 ( $CD_0$ ) and at L/P = 1300 ( $CD_{1300}$ ), given with equation  $CD_{LC} = 0.74 CD_0 + 0.26 CD_{1300}$ .

Upon the adsorption, aSyn assumes an  $\alpha$ -helical confirmation<sup>33</sup>. In Figure 4.1a we are showing CD spectra of aSyn in the absence and presence of vesicles containing 30% of PS lipids. The characteristic CD spectra of an  $\alpha$ -helix has a minimum at  $\lambda = 222$  nm, as is illustrated in Figure 3.6. It is then evident that by increasing lipid concentration the amount of  $\alpha$ -helices formed is also increasing. The increase of the amount of helices formed with increasing lipid concentration can be attributed to the larger lipid area accessible to aSyn to bind to.

In order to follow the amount of formed  $\alpha$ -helices we analysed the CD signal at 222 nm (Figure 4.1b) for samples of vesicles containing 30% and 50% of charged, PS, lipids. In both cases, saturation level, which is determined by the highest possible amount of  $\alpha$ -helices formed, is the same. However, when vesicles are containing more charged lipids, the saturation is reached at lower lipid to protein ratios. This can be attributed to stronger Columb attraction between positively charged aSyn monomers

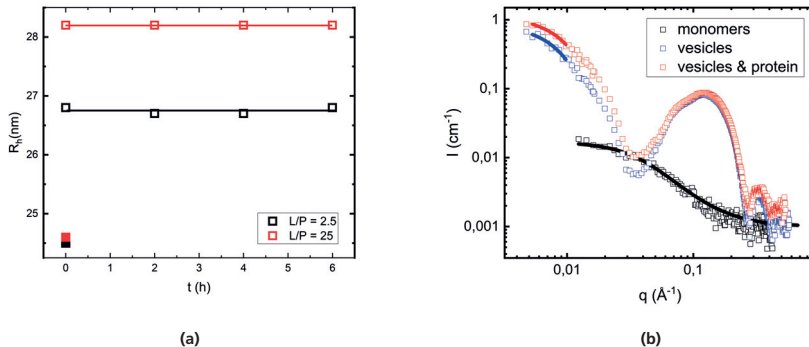


**Figure 4.2** (a) Hydrodynamic radius of vesicles in the absence (filled symbols) and presence (open symbols) for  $L/P = 2.5$  (red) and  $L/P = 25$  (black). All experiments were performed at pH 7.0. (b) Scattering profiles of aSyn monomers at  $140 \mu\text{M}$  protein concentration (black open squares), pure vesicle dispersion at  $42 \text{ mM}$  lipid concentration (blue open squares) and sample containing vesicles and aSyn at  $L/P = 300$  (red open squares) at pH 7.0. The solid lines are representing models fitted to the data. Debye model (black line) was used to model monomer scattering. The best agreement with the data were for  $I(0) = 0.02 \text{ cm}^{-1}$  and  $R_g = 4 \text{ nm}$ . Guinier fit provided the best agreement with the data for  $I(0) = 0.9 \text{ cm}^{-1}$  in the case of vesicles (blue line), and for  $I(0) = 1.1 \text{ cm}^{-1}$  in the case of sample containing protein and vesicles (red line).

and negative charges present on the vesicle surface, which further implies that the adsorption is driven by electrostatic interactions.

It is also possible to reproduce the full CD spectrum by a linear combination of the spectra at  $L/P=0$  (only random coil) and at the plateau at high  $L/P$  (only  $\alpha$ -helix). In Figure 4.1c we show as an example curve of  $L/P=100$  which is in very good agreement with the linear combination of 26% of  $\alpha$ -helices and 76% of random coils. That it is possible to reproduce curve linear combination of random coils and  $\alpha$ -helices formed after saturation point means that there is no difference in  $\alpha$ -helices formed at  $L/P$  ratios before and above saturation point.

By means of DLS we can estimate the hydrodynamic radius of vesicles alone and vesicles with adsorbed protein. The data are shown in Figure 4.2a where we see that the adsorbed layer is ca. 2 nm thick. We can also conclude from this figure that in the time period of 6 h, there are no further changes in the hydrodynamic radius of vesicles coated with adsorbed protein.

We performed SAXS experiments on aSyn monomers, a pure vesicle dispersion and a sample containing vesicles and protein. In Figure 4.2b we are showing data for  $L/P = 300$ . According to the data shown in Figure 4.1b, we expect ca. 60% of aSyn molecules to be bound to vesicles at this condition. In Figure 4.2b, we are including the Debye model with  $R_{gp} = 4 \text{ nm}$  that was used to fit the monomer scattering, and Guinier models with  $I_v(0) = 0.9 \text{ cm}^{-1}$  and  $R_{gv} \approx 20 \text{ nm}$  and  $I_{vp}(0) = 1.1 \text{ cm}^{-1}$  and



$R_{gvp} \approx 20$  nm used to model the scattering of the protein-free sample (subscript  $v$ ) and the sample containing protein and vesicles (subscript  $vp$ ), respectively. The difference in intensities at  $q = 0$  is  $\Delta I(0) = I_{vp}(0) - I_v(0) = 0.2 \text{ cm}^{-1}$ . We attribute this excess scattering to the scattering of adsorbed aSyn monomers. We further conclude that the adsorption of monomers has no observable effect on the vesicle form factor. This implies that there is no observable deformation of the lipid vesicle, which is supporting the idea of the vesicle stability.

## Summary and conclusion

When aSyn monomers are mixed with POPC/POPS vesicles, aSyn adsorbs immediately onto the vesicle surface and adopts an  $\alpha$ -helical conformation. The maximum amount of  $\alpha$ -helices is the same when vesicles contain 30 and 50 percent of charged, POPS, lipids. The adsorbed aSyn layer is approximately 2 nm thick and the vesicles coated with aSyn are stable structures.

### 4.1.2 Reversible lipid disc micelle deformation

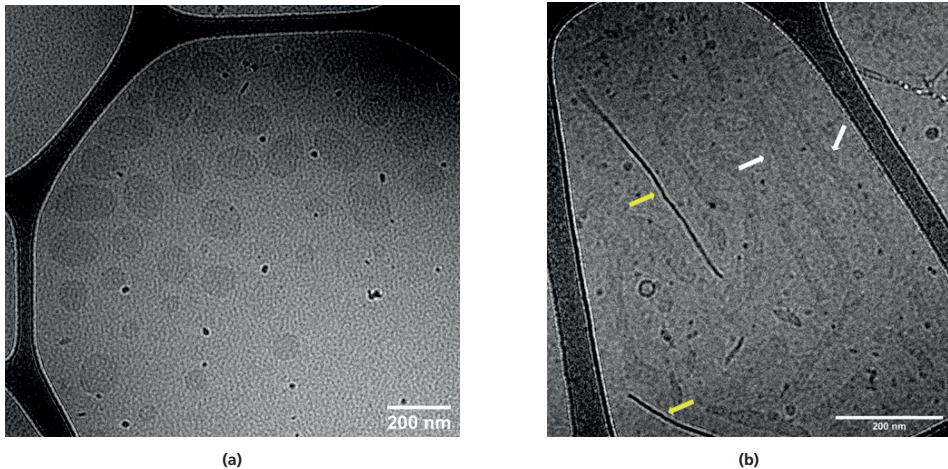


**Figure 4.3** (a) The pure lipid disc micelle dispersion. (b) Micelles after addition of aSyn. White arrows indicate elongated structures and yellow arrows indicate elongated structures whose normal is not perpendicular to the plane of view.

We investigated how the fibril formation affects the integrity of lipid disc micelles by means of cryo-TEM and SANS. The experiments were performed under conditions where the kinetics of fibril formation is sufficiently fast to happen in an experimentally accessible time frame. These conditions include slightly acidic pH of 5.5, a temperat-

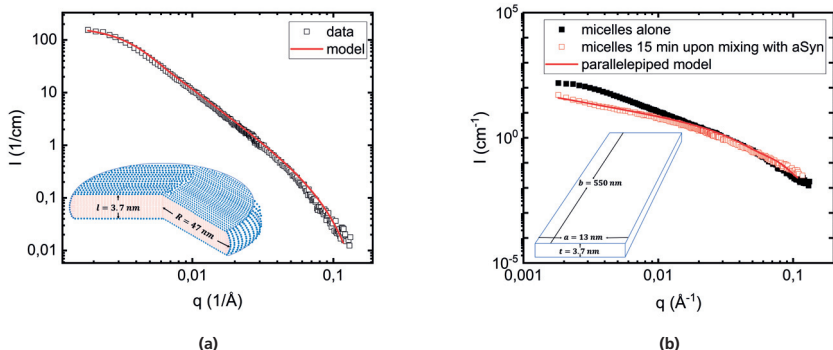


**Figure 4.4** (a) Scattering profile of the pure lipid disc micelle dispersion (black open squares) and the disc model that best fits the data (solid red line). As an inset we are showing an illustration of a lipid disc micelle with  $R = 47$  nm and  $t = 3.7$  nm. With red colour we are illustrating lipid chain region and with blue filled circles we are illustrating lipid head groups. (b) Scattering profile of pure disc dispersion (filled black squares), the scattering profile of discs in the first 15 minutes after addition of aSyn (open red squares) and the parallelepiped model used to fit the data (solid red line). The best model was obtained for length of shorter edge  $a = 13$  nm and length of longer edge  $b = 550$  nm, as illustrated in the inset.

ure of  $37^\circ\text{C}$  and the addition of pre-formed aSyn fibrils, so called-seeds. At pH 5.5, secondary nucleation, *id est* nucleation of formation of new fibrils on the surface of already formed fibrils, is a dominant process<sup>56</sup>, hence the addition of seeds accelerates the fibril formation. The data presented in this section are also given in Paper II.

In Figure 4.3 we show cryo-TEM images of pure disc micelle dispersion and disc that had just been mixed with aSyn. Prior to the addition of aSyn, disc micelles were almost circular, as is shown in Figure 4.3a. However, as shown in Figure 4.3b, addition of aSyn results in the remodelling of the disc micelles, which is concluded from the drastic changes in the disc morphology where originally circular lipid disc micelle assume highly elongated shape.

The SANS data are telling the same story. In Figure 4.4a we show the scattering pattern of the disc micelle dispersion. The data were successfully fitted with a disc model with length  $t = 3.7$  nm, corresponding to the bilayer thickness, and radius  $R = 47 \pm 14$  nm, as is shown in inset of Figure 4.4a. The comparison of the scattering profile of the pure disc dispersion and the scattering profile of discs 15 min after incubation with aSyn is shown in Figure 4.4b. The difference in the profiles is evident in the low  $q$ -region, where the power law dependence of  $I(q) \sim q^{-2}$ , which fitted the data for disc micelles alone, is changed to  $I(q) \sim q^{-1}$ . The  $I(q) \sim q^{-1}$  is a scattering signature of elongated structures, which is in agreement with what is seen in Figure 4.3b. The scattering profile obtained during the first 15 minutes of incubation was fitted with a parallelepiped model that in Figure 4.4b is shown as a red solid line.

An illustration of the parallelepiped is shown as an inset in the same figure. The best agreement with the data was obtained for a very long parallelepiped with height  $t = 3.7$  nm, width  $a = 13$  nm and length  $b = 550$  nm.

Initially, disc micelles are circular objects composed of 2 regions: the flat part and the curved rim. Due to the significant difference between these two parts, disc micelles are often composed of two different molecules, one preferring the flat and the other preferring the curved part. We believe that in the case of DMPC/DMPS lipids, it is the charged, DMPS, lipid molecules that prefer to be located in the curved region due to the electrostatic contribution to the monolayer spontaneous curvature<sup>91</sup>. However, there is an excess of DMPS lipids, which means that they also populate the flat part of lipid disc micelles. As the curved are increases and the flat area decreases upon aSyn adsorption, we conclude that aSyn has a preference to adsorb at the highly curved rim.

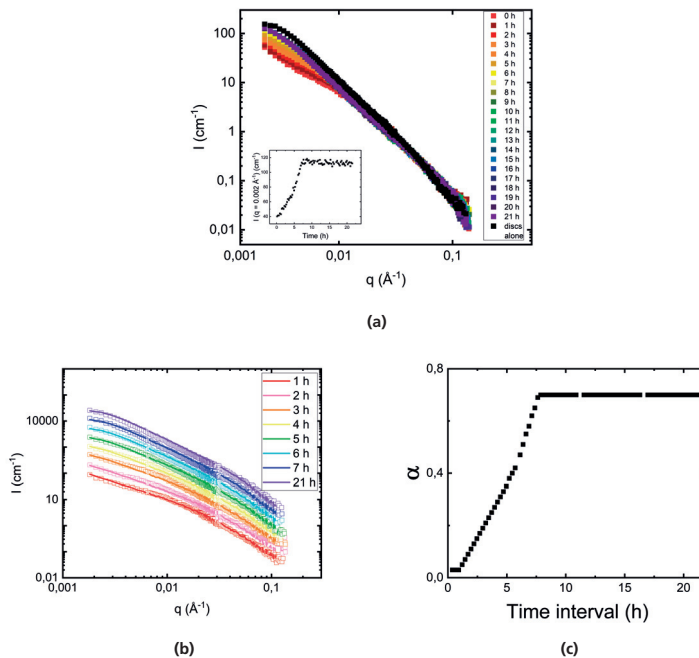


**Figure 4.5** (a) Time resolved SANS profiles,  $I(q)$  vs.  $q$ , plotted for a total time period of ca. 22 h. with a time resolution of 1 h. (b) Scattering profiles obtained at different time points (open squares) were modelled as a superposition (solid lines) of scattering profile obtained during the first 15 minutes after mixing and the pure disc dispersion. (c) The fraction of recovered circular micelles versus time.

The time evolution of scattering profile is shown Figure 4.5a. The recovery to almost initial shape is evident ca. 8 h of the incubation of aSyn and lipid disc micelles. Inter-

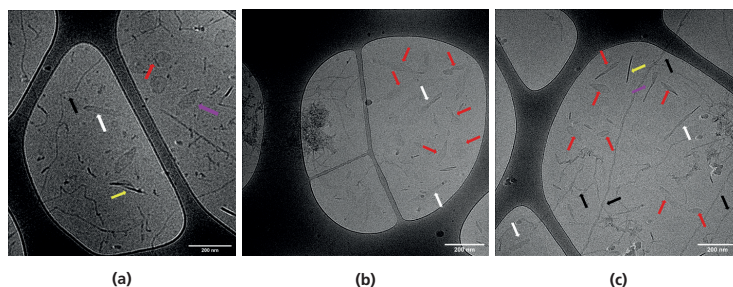


**Figure 4.6** Cryo-TEM images taken: (a) 3 h after mixing, (b) 7 h after mixing and (c) 21 h after mixing. White arrows indicate elongated structures, yellow arrows indicate structures whose normal is not perpendicular to the plane of view, pink arrows indicate partially recovered structures, red arrows indicate recovered structures and black arrows indicate aSyn fibrils.

estingly, a linear combination of pure disc micelle scattering,  $I_d$  and micelle scattering  $I_5$  after mixing, which is approximated with parallelepiped scattering,  $I_{par}$ , is providing a good agreement with the data obtained after 30 min of incubation and at the later time points. Some selected results of these analyses are shown in Figure 4.5b. The solid lines in the Figure are calculated via the equation  $I(q) = \alpha I_d + (1 - \alpha) I_{par}$ , where  $\alpha$  is the fraction of circular disc micelles and  $(1 - \alpha)$  is the fraction of elongated micelles. In Figure 4.5c we have plotted the obtained  $\alpha$  values as a function of time. As can be seen,  $\alpha$  reaches a steady state value of 0.7 after ca. 8 h, which means that 70 % of the micelles recover to their original circular shape and 30 % remain elongated.

The co-existence of recovered and remodelled micelles, which can be concluded from the SANS analyses, was also confirmed by cryo-TEM imaging. In Figure 4.6 we display images taken at different time points of incubation of aSyn and disc micelles. It is evident from the figure that elongated and circular discs co-exist during the fibril formation.

The recovery can be explained by desorption of aSyn monomers from the disc surface and incorporation in the newly formed fibrils. The co-existence of elongated and circular discs indicates a non-or-all type of behaviour and is consistent with recent findings of highly cooperative adsorption<sup>92</sup>.

## Summary and conclusions

The conclusions from this work can be summarised in a cartoon presented in Figure 4.7. There we illustrate fast adsorption of aSyn monomers onto the lipid disc micelles during which aSyn assumes  $\alpha$ -helical conformation. Upon the adsorption, disc micelles undergo through morphological changes from almost circular to the highly elongated structures, which can be modelled as long parallelepipeds. The process of

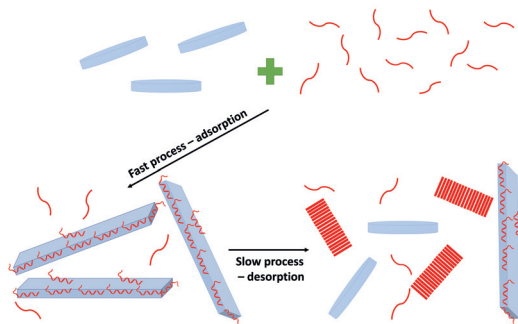


**Figure 4.7** A schematic illustration of the main findings. Top: circular lipid disc micelles (blue) are incubated with aSyn monomers (red). Bottom left: adsorption of aSyn monomers onto disc micelles is a fast process that results in a formation of elongated structures that can be approximated with parallelepipeds. Bottom right: aSyn desorption is a cooperative and slow process that results in a recovery of discs to their original shape.

monomer desorption and their incorporation into the fibrils is a cooperative process, which is more slow than the monomer adsorption. After all the monomers have been desorbed from the surface of one disc, it recovers to its initial circular shape.

#### 4.1.3 Fibril formation from the membrane's perspective: vesicle fusion

As membrane disruption has been proposed to be one of the mechanisms of cell death in PD, we looked at the end state of fibril formation when fibrils are formed in the presence of lipid vesicles. Lipid vesicles were composed of a combination of two phospholipids, zwitterionic POPC and anionic POPS, standing in POPC/POPS = 7/3 molar ratio and the samples were prepared at pH = 6.0, 6.5, 7.0 and 7.4 at L/P = 7.5. We performed cryo - TEM experiments and contrast matching SANS scattering experiments using deuterated aSyn and protonated lipids in D<sub>2</sub>O, which resulted in contrast matching of the protein. Both experiments are indicative of vesicle fusion. The data discussed in this section are also presented in Paper II.

From the analyses of the cryo - TEM data presented in Figure 4.8 we conclude that the fibril formation in the presence of POPC/POPS vesicles results in an increase in the vesicles size of ca. 3 fold. The SANS data shown in Figure 4.9 are confirming the increase in the vesicle size observed by cryo - TEM, through the increment of the scattering intensity for  $q < 0.006 \text{ \AA}^{-1}$ . However, we are unable to make conclusions about how much exactly has the size increased as we are lacking the Guinier regime in the SANS data coming from samples containing vesicles in the presence of fibrils.

However, the conclusion that can be drawn from the SANS data are that the bilayer concentration remains constant, which is concluded from the overlap of scattering

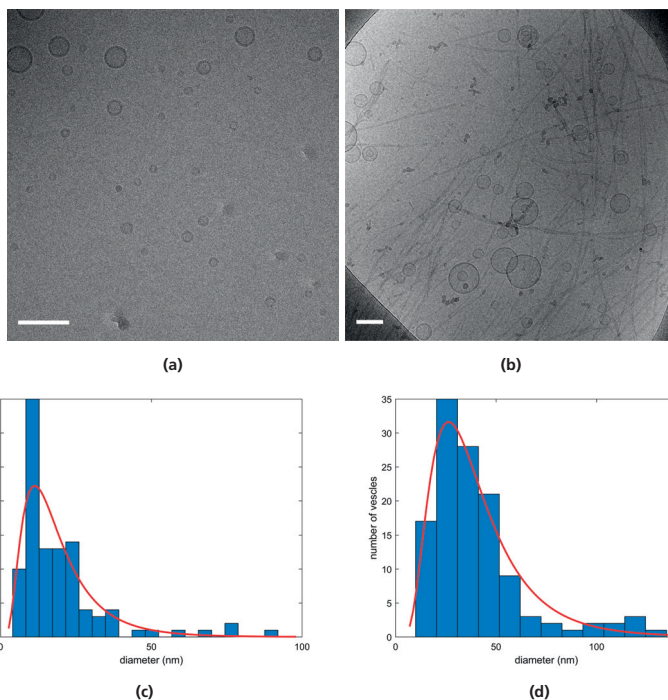


**Figure 4.8**  $\text{pH} = 6.0$ : Cryo-TEM image of pure vesicles dispersion at  $c_L = 2.1$  mM (a) and vesicles in the presence of fibrils at  $L/P=7.5$  (b). The scale bar corresponds to 100 nm. Size distribution of vesicle diameter obtained from cryo-TEM images, in the case of pure vesicle dispersion (c) and vesicles in the presence of fibrils (d). The red line is the fit by log-normal distribution.

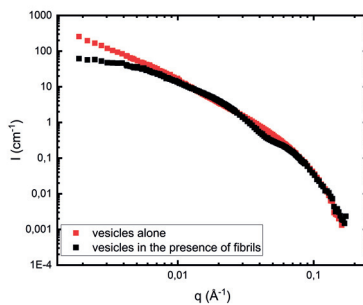


**Figure 4.9** Comparison of scattering profiles of pure vesicle dispersion (black squares) and vesicles in the presence of fibrils (red squares) at  $\text{pH} 6.0$ , measured at  $20^\circ \text{C}$ .

patterns at high  $q$ . The conserved concentration of the bilayer implies that there is no observable extraction of lipids from the membrane, which is one of the proposed mechanisms for membrane disruption.

## Summary and conclusion

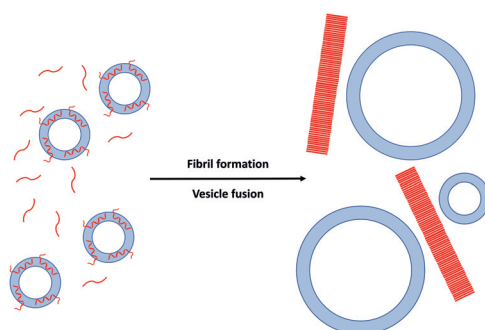


**Figure 4.10** A schematic illustration of the fusion of POPC/POPS vesicles during aSyn fibril formation. The vesicles coated with aSyn monomers are stable structures. However, fibril formation can be induced by addition of seeds. Some time during the fibril formation, some of the vesicles fuse together.

The observed scenario of the vesicle fusion is schematically illustrated in Figure 4.10. As was seen in section 4.1.1, vesicles with adsorbed aSyn monomers at pH 7.0 are stable structures. However, when the fibril formation is induced by addition of pre-formed fibrils, some of the vesicles undergo a fusion event.

How, when and why fusion events occur we are unable to tell based on the current data. However, the vesicles observed at the later stage, *id est*, after the fibril formation took place, appear to be stable, which means that the fusion events are already finished. The fact that we only see increase for ca. factor of 3 and that we roughly reproduce the vesicle size increase at 4 pHs investigated (the rest of the data shown in Paper II), indicates that fusion events are not taking place in the presence of mature fibrils, but rather at early stages of the fibril formation. What we presume is that the vesicle fusion happens during the desorption of monomers from the vesicle surface and their incorporation inside fibrils.

### 4.1.4 Fibril formation from the protein's perspective: no observable co-assembly formation on the molecular length scale

Amyloid fibrils are long, unbranched structures with radius between 5 and 14 nm<sup>93</sup>. They are characterised by so-called cross- $\beta$  structure, which involves  $\beta$ -sheets that run parallel to the fibril axis and  $\beta$ -strands perpendicular to the axis. The  $\beta$ -sheets are intermolecular and each monomer is composed of several  $\beta$ -strands. The protein monomers are folded in 2D and then stacked in the third dimension, the fibril direction.

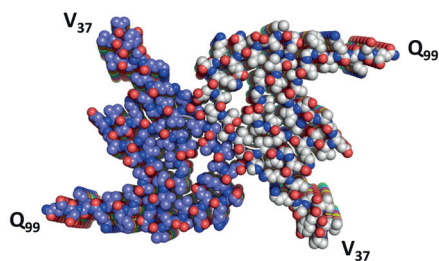


**Figure 4.11** A PDB structure (6A6B) of aSyn fibrils obtained from cryo-EM analysis, reported in 94. The PDB structure includes only residues comprising fibril core (V37-Q99). The two protofilaments are shown in different colours.

aSyn fibril structure has been investigated by solid-state NMR (ss-NMR)<sup>95,96</sup> and cryo-TEM<sup>94,97,98</sup>. All of the structural models that reproduce the data show that aSyn fibrils are composed of two intertwined protofilaments. Each protofilament is forming one  $\beta$ -sheet. It has also been shown that it is not the entire aSyn molecule that assumes ordered structure and composes fibril core, but rather only the middle 62 residues (from 37<sup>th</sup> to 99<sup>th</sup>)<sup>94</sup>. An X-ray scattering study performed by Pogostin *et al.* showed that the radius of aSyn fibrils equals to 5.2 nm and that the higher order arrangements of fibrils is pH dependent<sup>71</sup>. In Figure 4.11 we are showing PDB structure of aSyn fibrils taken from<sup>94</sup>. The PDB structure shows only 62 residues that are comprising the fibril core.

The data discussed in this section are also presented in Paper III. In this work, we have investigated aSyn fibrils formed in the presence and absence of lipid membranes by means of X-ray scattering. X-ray scattering experiments yield information about both the cross-section dimension and the  $\beta$ -strand repeat distance. The cross-section dimension follows from the small-angle regime, whereas the  $\beta$ -strand repeat distance follows from the wide-angle regime. In order to address possible co-assembly formation, we investigated fibril cross-section dimension and cross- $\beta$  structure when fibrils were formed in the presence of model membranes. The model membranes were vesicles composed of POPC and POPS lipids, standing in molar ratio POPC/POPS = 7/3. Experiments were performed at pH 6.0, 6.5 and 7.0 at a protein concentration of 280 $\mu$ M and varying lipid concentrations (the rest of the data is presented in Paper III).

In Figure 4.12 we show the scattering profile of POPC/POPS vesicles. As the average SLD of these vesicles is almost equal to that of water, the contribution to scattering



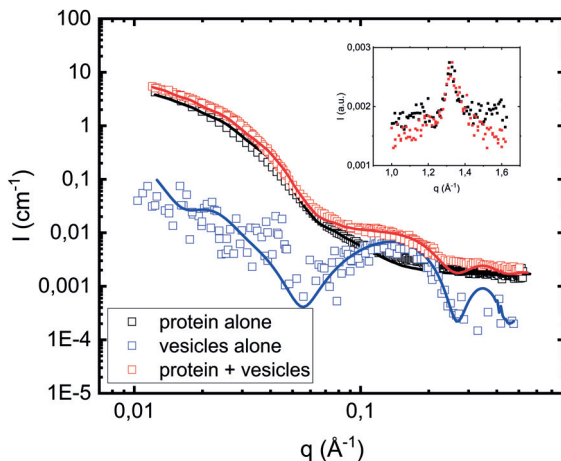


**Figure 4.12** Scattering profiles of fibrils formed in the absence of vesicles at a protein concentration of  $280 \mu\text{M}$  at pH 6.0 (empty black squares), pure vesicles dispersion at pH 6.6 and at 2.1 mM lipid concentration and LP=7.5 (empty blue squares) and fibrils formed in the presence of vesicles at pH 6.0 and LP=7.5 (empty red squares). The solid black line is the simulated scattering pattern based on the cylinder model, the solid blue line is the simulated scattering pattern based on the core–multi–shell model and solid red line is the best fit with the linear combination of the cylinder and core–multi–shell models. As an inset, the wide–angle diffraction pattern with a peak at  $q = 1.3 \text{ \AA}^{-1}$  is shown in the case of fibrils formed in the absence of lipids (black symbols) and fibrils formed in the presence of lipids (red symbols).

at low  $q$  is negligible. The only contribution to the scattering profile is a broad maximum around  $q = 0.15 \text{ \AA}^{-1}$ , reporting on the SLD profile across the bilayer. As the contribution to the scattering profile is from the bilayer, we modelled the vesicle scattering profile with a core–shell model (Eq: 3.15), composed of 3 shells: two outer shells representing the head group layers and the inner shell representing the acyl chain layer. The fit is shown as blue line in Figure 4.12.

Using the advantage that POPC/POPS vesicles are well matched in water when scattering with X-rays, we compared scattering profiles of fibrils formed in the absence and presence of lipid vesicles, as shown in Figure 4.12. Fibrils formed in the absence of lipid vesicles were successfully fitted with the cylinder model (Eq. 3.14) with radius equal to 5.2 nm, in agreement with what has previously been reported in<sup>71</sup>. The scattering pattern of fibrils formed in the presence of vesicles can be compared to that of the fibril formed in the pure buffer, apart from the additional broad hump around  $q = 0.15 \text{ \AA}^{-1}$ . As is seen in the scattering pattern of the vesicle dispersion, the hump is a consequence of the lipid bilayer scattering.

The fitting of scattering profile of fibrils formed in the presence of lipids was success-

fully performed with a linear combination of the cylinder model describing the fibrils formed in the pure buffer and the core multi-shell model describing the lipid bilayer. The model parameters correspond to ones used to model pure fibril and bilayer scattering. That the data were fitted with the linear combination of cylinder and core-shell sphere implies that the cylinder cross-section and the bilayer dimensions are the same as in the pure fibril and pure vesicle samples.

In the inset of Figure 4.12 we show the peak at  $q = 1.3 \text{ \AA}^{-1}$  which is a signature of the cross- $\beta$  structure. The peak is present both in fibrils formed in the absence and the presence of vesicles, which implies that the  $\beta$ -strand distance is unaffected by the presence of lipids during fibril formation.

### Summary and conclusions

Comparing SAXS patterns of aSyn fibrils formed in absence and presence of POPC/POPS lipid vesicles does not reveal any difference in the fibril cross-section size and shape. This further suggests that the presence of lipids during fibril formation does not lead to any significant unfolding or change in the packing of the protein molecules in the fibrils. By comparing wide-angle patterns, we conclude that the  $\beta$ -strand repeat distance,  $d_\beta = 4.7 \text{ \AA}$ , is unaffected by the presence of lipids during the fibril formation. Both small and wide-angle data indicate that there is no observable mixing of lipid and protein on the molecular length scale. We also conclude that there is no impact on the area per lipid molecule in the bilayer membrane.

## 4.2 Part II: Arrangements of colloiddally unstable aSyn fibrils

The role of LBs in PD is not fully understood. Moreover, it has been proposed that LB formation is not the cause of the disease, but rather a way to deposit damaged cellular components and misfolded fibrils<sup>99,100</sup>. Nevertheless, it is crucial to understand LB structure and pathways to LB formation, as it is well known that these inclusions are present in brains of PD patients.

First ultrastructural characterisation of LBs was done by Duffy and Tennyson in 1965 using phase contrast and electron microscopy<sup>101</sup>. They studied 102 LBs and found that they differ in morphology. The “simple LBs”, as they call them, are composed of a dense core and less dense zone, whereas more complex LBs are multilamellar and have outer zones of different densities. Both dense core and outer zone are composed of filaments, which are radially oriented in the outer zone and more densely packed in the dense core. The nature of these filaments remained a mystery for more than 30 years after the first characterisation of LBs. It was finally determined in 1998 that the aggregated form of aSyn composes the filamentous structure in LBs<sup>20,21</sup>. Apart from aSyn, LBs contain various lipids and cell organelles<sup>22-24,101,102</sup>, that seem to be trapped into clusters formed by aSyn fibrils.

### 4.2.1 Colloiddally unstable aSyn fibrils are arranged into mass fractal clusters

We have investigated the behaviour of aSyn fibrils formed at pH 5.5, close to their isoelectric point ( $pI \approx 4.8$ <sup>69,103</sup>). At these conditions, the fibrils are not sufficiently charged to be colloiddally stable and they aggregate further into dense clusters. We investigated these clusters by means of the SANS technique. We performed SANS measurements on 19 samples that are for simplicity numerically labelled and described in the Table 4.1. There is a small difference in the sample preparation. Fibrils were formed by incubating monomers obtained from SEC in a pure 10 mM MES buffer (samples 1, 5 and 8) or in the presence of lipid vesicles (remaining 16 samples). Samples 1-4 were prepared using deuterated protein and sample 5-19 using protonated protein. 2 min centrifugation at 6720 rcf was performed on samples 1-4 and 15 min centrifugation at 15615 was performed 5 times on samples 8-19. The centrifugations resulted in the formation of a dense pellet. After each centrifugation step, the supernatant was separated from the pellet. The removal of the supernatant was done in order to minimise the impact on the scattering profile from lipid molecules that were not part of the aggregates and hence did not sediment during the centrifugations. Samples 5-7 were dialysed against 100% D<sub>2</sub>O buffer overnight with the aid of a dialysis membrane having  $M_w$  cut of 3500 kDa. The data presented in this section

are found in Paper IV.

In Figure 4.13 we show scattering profiles of all 19 samples. The results are strikingly similar for all the samples investigated, regardless of sample preparation. All scattering profiles are showing a simple power-law behaviour,  $I(q) \sim q^{-d}$ , where  $d$  can be considered as a fractal dimension of the clusters. The variation of the fractal dimensions of all 19 samples is shown as an inset in Figure 4.13. The mean value of the fractal dimension occurring in all 19 samples equals to  $2.6 \pm 0.3$ . The fractal dimension in this range is indicative of mass fractals. Data shown in Figure 4.13 were recorded using rotating sample cells to prevent macroscopic sedimentation.

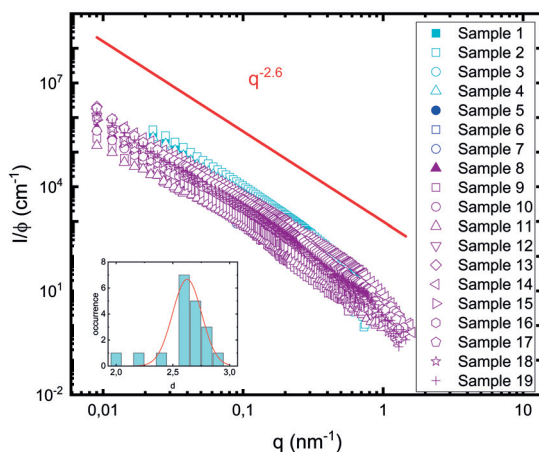


**Figure 4.13** The scattering profiles of 19 samples presented on the absolute scale, normalised by protein volume fraction. The samples containing lipids are represented with open symbols. Samples 1-4 are shown in cyan, samples 5-7 are shown in blue and samples 8-19 are shown in purple. Samples containing protein alone are represented with filled symbols. For comparison, as a red line is shown a power law dependence of the scattering intensity on  $q$ -vector, with power value equal to  $2.6 \pm 0.3$ .

Three characteristic regimes are expected in the scattering profile of mass-fractal clusters of hard rods if a wide enough  $q$ -range is covered in experiments<sup>104</sup>. The so-called Guinier regime is present at low  $q$ -values, *id est* for  $q < 1/R_g$ . At intermediate  $q$ -values, for  $1/R_g < q < 1/\xi$ , where  $\xi$  is the cluster mesh-size, the scattering intensity takes a power law dependence on the scattering vector,  $I(q) \sim q^{-d}$ . Finally, for  $q > 1/\xi$ , scattering intensity is the form factor of a rod,  $I(q) \sim q^{-1}$ . In our data, we do not observe a Guinier regime, which implies that the clusters are too big for the investigated  $q$ -range. We also do not observe  $I(q) \sim q^{-1}$ , which implies that the cluster mesh-size is too small, approximately of the same order as the fibril diameter. For finite diameter rods there is in addition the Porod region at high  $q$  with

$$I(q) \sim q^{-4}.$$

**Table 4.1** Summary of 19 samples investigated by SANS. The table shows the protein and lipid concentration, lipid composition in the model membranes and the deuteration level of the buffer used in the scattering experiment.

Sample number	Protein isotope and concentration	Buffer composition	Lipid composition	Lipid to protein molar ratio
1	d-aSyn, 110 $\mu$ M	100 % H <sub>2</sub> O	–	–
2	d-aSyn, 110 $\mu$ M	100 % H <sub>2</sub> O	DOPC/DOPS	1
3	d-aSyn, 110 $\mu$ M	100 % H <sub>2</sub> O	DOPC/GM1	1
4	d-aSyn, 110 $\mu$ M	100 % H <sub>2</sub> O	DOPC/GM3	1
5	h-aSyn, 140 $\mu$ M	100 % D <sub>2</sub> O	–	–
6	h-aSyn, 140 $\mu$ M	100 % D <sub>2</sub> O	DOPC/DOPS	0.4
7	h-aSyn, 140 $\mu$ M	100 % D <sub>2</sub> O	DOPC/GM1	0.4
8	h-aSyn, 140 $\mu$ M	100 % D <sub>2</sub> O	–	–
9	d-aSyn, 110 $\mu$ M	100 % H <sub>2</sub> O	DMPC/DMPS	1
10	h-aSyn, 140 $\mu$ M	100 % D <sub>2</sub> O	DMPC/DMPS	5
11	h-aSyn, 140 $\mu$ M	100 % D <sub>2</sub> O	DMPC/DMPS	15
12	h-aSyn, 140 $\mu$ M	100 % D <sub>2</sub> O	POPC/POPS	1
13	h-aSyn, 140 $\mu$ M	100 % D <sub>2</sub> O	POPC/POPS	2
14	h-aSyn, 140 $\mu$ M	100 % D <sub>2</sub> O	POPC/POPS	5
15	d-aSyn, 110 $\mu$ M	100 % H <sub>2</sub> O	POPC/GM1	1
16	h-aSyn, 140 $\mu$ M	100 % D <sub>2</sub> O	POPC/GM1	2
17	h-aSyn, 140 $\mu$ M	100 % D <sub>2</sub> O	POPC/GM1	5
18	h-aSyn, 140 $\mu$ M	100 % D <sub>2</sub> O	POPC/GM3	1
19	h-aSyn, 140 $\mu$ M	100 % D <sub>2</sub> O	POPC/GM3	2

With the goal to better understand the fibril cluster organisation, we have constructed models of fibril clusters, as described in section 3.1.3. In order to investigate different cluster arrangements, we modelled clusters where each fibril is connected to the previous one at a random monomer position and clusters where each fibril was connected with its middle monomer to a randomly chosen monomer of the previous fibril. We have also compared our models with a well-known model of freely-jointed chain (FJC), where each fibril is connected end-to-end. The scattering of the FJC corresponds to the scattering of a polymer chain, and as such is well described by the Debye model given by Eq. 3.11. Comparisons between different calculated cluster form factors is shown in Figure 4.14.

All three regimes expected for the scattering of a mass fractal are evident in Figure 4.14. By using the Beaucage model (Eq. 3.13) to fit the mass clusters where fibrils were connected at random or middle positions, and the Debye model (Eq. 3.11) to fit FJC clusters, we were able to deduce the fractal dimension and the radius of gyration of these model clusters. In the case of randomly connected fibrils, the Beaucage model

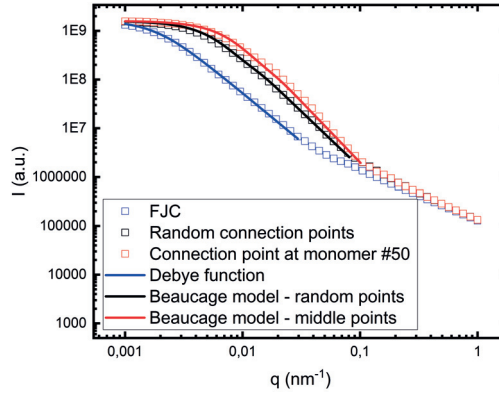


**Figure 4.14** Comparisons between different calculated cluster form factors: (i) FJC model (blue open squares), (ii) random connection points (black open squares), and (iii) each fibril having one connection point at the middle monomer (red open squares). The blue solid line in (i) correspond to a model calculation using the Debye function (Eq. 3.11). The black and the red solid lines correspond to model calculations using the Beaucage model (Eq. 3.13).  $R_g$  decreases and  $d$  increases from (i) to (iii).

gives  $R_g = 300$  nm and  $d = 2.3$ . For clusters where fibrils are connected in the middle, the best fit with the Beaucage model gives  $R_g = 220$  nm and  $d = 2.5$ . The Guinier scaling factor was the same in both cases and equal to  $G = (N_{fib}N_{mon})^2 = 1.610^9$ , where  $N_{fib}$  and  $N_{mon}$  are total number of fibrils and monomers in the clusters, respectively. Fitting FJC clusters with the Debye model gives  $R_g = 808$  nm. From the analysis shown in Figure 4.14 it is obvious that by lowering the average “step-length”, which in our case is the average separation between the two monomer positions within a fibril that are shared with other fibrils, we are producing more densely packed clusters described by higher  $d$  and lower  $R_g$  values.

## Summary and conclusions

aSyn fibrils formed at pH 5.5 aggregate further into dense fibril clusters that are prone to sedimentation. This fibrillar arrangement is different from one that aSyn fibrils assume at higher pH<sup>71</sup>. As the fibril clusters formed at pH 5.5 resemble the fibrillar network seen in LBs, we analysed these cluster in more detail. The observed arrangement can be explained by the presence of attractive interaction. The origin of these attractive interactions is most likely hydrophobic, as the presence of extended hydrophobic cores has been reported in aSyn fibrils<sup>94,97,105,106</sup>.

We learned that the clusters are arranged in mass fractals with fractal dimension of

$d = 2.6 \pm 0.3$  and that the fractal dimension is independent on differences in the sample preparation. We also constructed a simple model of rigid-rod clusters to further confirm the conclusion observed experimentally. The model, that can be regarded as the extension of FJC model of flexible polymers, was able to reproduce the fractal dimension observed experimentally.

#### 4.2.2 Sedimentation of the fibril clusters influences the rate of fibril formation

As discussed above, aSyn fibrils are not colloidally stable at pH 5.5, but aggregate further into dense clusters that are prone to sedimentation. This has consequences for fibril formation. At pH 5.5 secondary nucleation of fibrils is rapid and the dominant nucleation mechanism<sup>56</sup>. If samples are not stirred or rotated, formed fibrils are sedimenting out of solution, reducing the available surface for the secondary nucleation. This results in a significant reduction of the fibril formation rate, possibly even a temporary termination. Thus, working at this pH requires well defined and strict experimental protocols.

In Figure 4.15 we are demonstrating the influence of stirring during the fibril formation process on the amount of formed fibrils. In Figure 4.15a, we are showing photographs of samples containing aSyn fibrils and POPC/POPS vesicles. The samples are milky and sedimenting and the amount of fibrils is significantly higher when stirring was employed. In Figure 4.15b we show a dense pellet that is formed after centrifugation of the samples.

We also performed SAXS experiments on the supernatants removed above the pellets formed during centrifugation when the fibril formation was performed under quiescent and stirring conditions. The results shown in Figure 4.15c imply that there is protein present in the supernatant when there was no stirring applied. In the case where the stirring was applied during the fibril formation, the supernatant is empty, which means that most of aSyn monomers are incorporated in the fibrils. The SAXS data from the supernatant removed from sample prepared under quiescent conditions was fitted using the Debye form factor (Eq. 3.11) with  $R_g = 3.5$  nm and  $I(0) = 0.076$  cm<sup>-1</sup>. The  $I(0) = 0.076$  cm<sup>-1</sup> corresponds to the scattering of aSyn monomers at 350  $\mu$ M, which is higher than (280  $\mu$ M) the initial concentration of aSyn monomers used in this experiment. This further implies that the supernatant contains particles with higher molecular weight, dimer, trimer, etc.

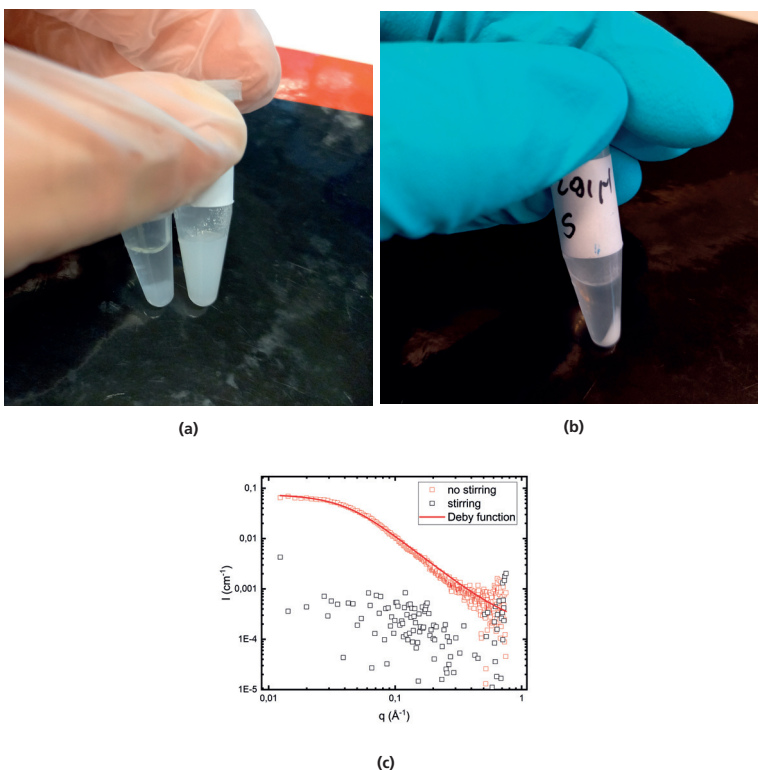


**Figure 4.15** (a) The photographs taken of samples after the incubation period, when fibrils were formed under quiescent conditions (left) and under stirring (right). The protein fibrils were produced by incubating  $280\mu\text{M}$  of aSyn monomers and vesicles composed of POPC/POPS lipids, at lipid to protein ratio  $L/P=2.5$ . (b) The pellet formed during centrifugation when stirring was introduced during fibril formation. (c) Scattering profiles of supernatants removed when fibrils were formed under quiescent conditions (open red squares) and under stirring (open black squares). Protein concentration equals to  $280\mu$  and  $L/P=2.5$ . Scattering profile of supernatant removed from samples formed under quiescent conditions was fitted with Debye function with  $I(0) = 0.76\text{ cm}^2$  and  $R_g = 3.5\text{ nm}$ .

## Summary and conclusions

aSyn fibrils formed at pH 5.5 arrange into sedimenting fibril clusters. When stirring is introduced during fibril formation, aggregation kinetics is significantly faster compared to one occurring under quiescent conditions. We explain this observation by loss of catalytic surface for the new fibrils to form. As the secondary nucleation process is a dominant process at this pH<sup>56</sup>, the precipitation of fibrils has a big effect on the kinetics of fibril formation.



### 4.2.3 Lipids co-sediment with fibril clusters

As LB are agglomerates, composed of various lipids<sup>22-24</sup> and membrane organelles<sup>101, 102</sup>, seemingly trapped in the cluster of aSyn fibrils, it is highly likely that aSyn fibrils trap other LB components while collapsing. As a way to address this possibility, we made use of the sedimentation of aSyn clusters, invoking also centrifugation, and investigated whether lipid vesicles are co-sedimenting with fibrils.

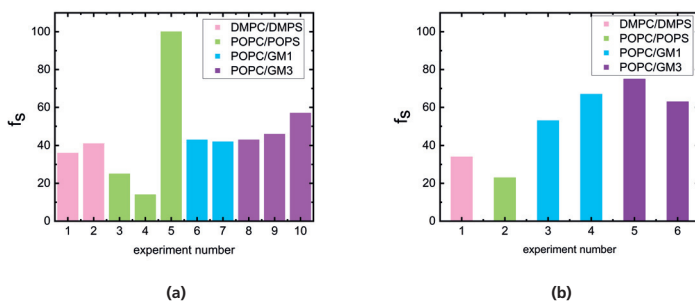


**Figure 4.16** Fractions of lipids sedimenting relative to the initial lipid amount for different lipid systems. Pink colour is representing DMPC/DMPS lipids, green colour is representing POPC/POPS lipids, blue colour is representing POPC/GM1 lipids and purple colour is representing POPC/GM3 lipids. ASyn concentration was equal to  $280\mu\text{M}$  and lipid to protein ratio was equal to 2.5. (a) Fibrils were formed under quiescent conditions. (b) Fibrils were formed under stirring.

In Figure 4.16 we show results of the NMR experiments performed in order to measure lipid concentration in supernatants. As can be seen, lipids sediment together with aSyn fibrils. However, the amount of sedimenting lipids is not reproducible.

We were also looking into ratio of charged/neutral lipids that are sedimenting and found that the percentage of gangliosides sedimenting is higher than the percentage of POPC lipids when vesicles were composed of 90% POPC lipids and 10% gangliosides. We found that ca. 35% of total POPC lipids is sedimenting, and 60% of total gangliosides. The observed selectivity implies existence of attractive interactions between membranes and fibrils.

### Summary and conclusions

When aSyn fibrils are formed in the presence of lipid membranes at pH 5.5, the sedimentation of dense fibril clusters also results in the sedimentation of lipids. However, we are not able to say whether the co-sedimentation is due to attractive fibril-membrane interactions or if the membranes are trapped in the sedimenting network of aSyn fibrils, or if it is interplay between the two.



# Epilogue

In this thesis we have studied the interactions between model lipid membranes and monomers and fibrils of the protein  $\alpha$ -Synuclein (aSyn), that is associated with Parkinson's disease. The main results have been summarised and discussed above. Obviously, much more work is needed in order to fully understand these very important systems. Below I suggest some further work that possibly can build on the results, conclusions and ideas of this work.

1. As our studies presented in Paper II and III are limited to a particular lipid system, it would be useful to extend the studies to other lipid systems in order to address the question of generality or possible selectivity. The additional experiments that could be performed are quantitative analyses of monomer adsorption and vesicle stability, as well as the investigation of the possible effect that presence of lipids during fibril formation has on the fibril structure.
2. We observed fusion of lipid vesicles at the course of fibril formation. However, we are unable to say when, how and why fusion events occur. In order to answer these questions, we need to perform time resolved experiments using different techniques. Some of the techniques that could be used to gain insight in the fusion events are time resolved contrast matching SANS experiments, where we would match the protein and follow changes in vesicle scattering profile, similar to what we did with disc micelles in Paper I. One may also consider time resolved NMR, for example  $^{31}\text{P}$  or  $^1\text{H}$  NMR relaxation, which can provide information on the vesicle size. Also time resolved diffusion NMR could be useful to follow possible changes in vesicle size and/or interactions with fibrils. Furthermore, time resolved imaging techniques, for example cryo-TEM, could also be used.
3. In Papers IV and V we made a first attempt to address the formation of Lewy bodies from the point of view of attractive aSyn fibril-fibril interactions. Is a mildly acidic pH involved, or are there other factors in vivo that can induce effectively attractive interactions? For example, by altering the molecular packing in the aSyn fibrils, making them increasingly hydrophobic. Thus, it could be important to investigate in more detail the aSyn fibril structure under different conditions.



# References

- [1] Berg, J. M.; Tymoczko, J. L.; Stryer, L. *Biochemistry Sixth Edition*; W.H. Freeman & Company, 2006.
- [2] Pace, C. N.; Scholtz, J. M.; Grimsley, G. R. Forces stabilizing proteins. *FEBS Letters* **2014**, *588*, 2177–2184.
- [3] Tompa, P. Intrinsically disordered proteins: a 10-year recap. *Trends in Biochemical Sciences* **2012**, *37*, 509–516.
- [4] Wright, P. E.; Dyson, H. J. Intrinsically Unstructured Proteins: Re-assessing the Protein Structure-Function Paradigm. *Journal of Molecular Biology* **1999**, *293*, 321–331.
- [5] Reynolds, N. P.; Adamcik, J.; Berryman, J. T.; Handschin, S.; Zanjani, A. A. H.; Li, W.; Liu, K.; Zhang, A.; Mezzenga, R. Competition between crystal and fibril formation in molecular mutations of amyloidogenic peptides. *Nature Communications* **2017**, *8*.
- [6] Baldwin, A. J.; Knowles, T. P. J.; Tartaglia, G. G.; Fitzpatrick, A. W.; Devlin, G. L.; Shammash, S. L.; Waudby, C. A.; Mossuto, M. F.; Meehan, S.; Gras, S. L.; Christodoulou, J.; Anthony-Cahill, S. J.; Barker, P. D.; Vendruscolo, M.; Dobson, C. M. Metastability of Native Proteins and the Phenomenon of Amyloid Formation. *J. Am. Chem. Soc.* **2011**, *133*, 14160–14163.
- [7] Adamcik, J.; Mezzenga, R. Amyloid Polymorphism in the Protein Folding and Aggregation Energy Landscape. *Angewandte Chemie International Edition* **2018**, *57*, 8370–8382.
- [8] Marshall, K. E.; Serpell\*, L. C. Insights into the Structure of Amyloid Fibrils. *The Open Biology Journal* **2009**, *2*, 185–192.
- [9] Astbury, W. T.; Dickinson, S.; Bailey, K. The X-ray interpretation of denaturation and the structure of the seed globulins. *Biochemical Journal* **1935**, *29*, 2351–2360.
- [10] Gertz, M.; Rajkumar, S. *Amyloidosis: Diagnosis and Treatment*; Springer, 2010.
- [11] O’Leary, E.; Lee, J. Interplay between  $\alpha$ -synuclein amyloid formation and membrane structure. *BBA - Proteins and Proteomics* **2019**, *1867*, 483–491.
- [12] Iadanza, M.; Jackson, M.; Hewitt, E.; Ranson, N.; Radford, S. A new era for understanding amyloid structures and disease. *Nature Reviews Molecular Cell Biology* **2018**, *19*, 755–773.

- [13] Parkinson, J. An Essay on the Shaking Palsy. *Sherwood, Neely and Jones* 1817,
- [14] Dauer, W.; Przedborski, S. Parkinson's Disease: Mechanisms and Models. *Neuron* 2003, 39, 889–909.
- [15] Poewe, W.; Seppi, K.; Tanner, C. M.; Halliday, G. M.; Brundin, P.; Volkman, J.; Schrag, A.-E.; Lang, A. E. Parkinson's Disease. *Nature Reviews Disease Primer* 2017, 3, 17013.
- [16] Fahn, S.; Sulzer, D. Neurodegeneration and neuroprotection in Parkinson disease. *NeuroRx* 2004, 1,, 139–154.
- [17] Bernheimer, H.; Birkmayer, W.; Hornykiewicz, O.; Jellinger, K.; Seitelberger, F. Brain dopamine and the syndromes of Parkinson and Huntington. Clinical, morphological and neurochemical correlations. *J Neurol Sci* 1973, 20,, 415–55.
- [18] Lewy, F. Paralysis Agitans. I. Pathologische Anatomie. *Handbuch der Neurologie* 1912, 920–33.
- [19] Tretiakoff, C. Contribution a l'etude de l'Anatomie pathologique du Locus Niger de Soemmering avec quelques deduction relatives a la pathogenie des troubles du tonus musculaire et de la maladie de Parkinson. Ph.D. thesis, Theses de Paris, 1919.
- [20] Baba, M.; Nakajo, S.; Tu, P.-H.; Tomita, T.; Nakaya, K.; Lee, V. M.-Y.; Trojanowski, J. Q.; Iwatsubo, T. Aggregation of  $\alpha$ -Synuclein in Lewy Bodies of Sporadic Parkinson's Disease and Dementia with Lewy Bodies. *American Journal of Pathology* 1998, 152, 879–884.
- [21] Spillantini, M. G.; Schmidt, M. L.; Lee, V. M. Y.; Trojanowski, J. Q.; Jakes, R.; Goedert, M.  $\alpha$ -Synuclein in filamentous inclusions of Lewy bodies from Parkinson's disease and dementia with Lewy bodies. *PNAS* 1998, 95, 6469–6473.
- [22] Fanning, S.; Selkoe, D.; Dettmer, U. Parkinson's disease: proteinopathy or lipidopathy? *The Nature Partner Journals Parkinson's Disease* 2020, 6.
- [23] Lashuel, H. A. Do Lewy bodies contain alpha-synuclein fibrils? and Does it matter? A brief history and critical analysis of recent reports. *Neurobiology of Disease* 2020, 141, 104876.
- [24] Stefanis, L.  $\alpha$ -synuclein in Parkinson's disease. *Cold Spring Harbor Perspectives in Medicine* 2012, 4, a009399.
- [25] Polymeropoulos, M. H. et al. Mutation in the  $\alpha$ -Synuclein Gene Identified in Families with Parkinson's Disease. *Science* 1997, 276, 2045–2047.
- [26] Spillantini, M. G.; Schmidt, M. L.; Lee, V. M. Y.; Trojanowski, J. Q.; Jakes, R.; Goedert, M. Alpha-synuclein in Lewy bodies. *Nature* 1997, 388, 839–840.
- [27] Chandra, S.; Chen, X.; Rizo, J.; Jahn, R.; Sudhof, T. A broken alpha -helix in folded alpha-Synuclein. *J Biol Chem* 2003, 278,, 15313–15318.
- [28] Burre, J.; Sharma, M.; Sudhof, T. C.  $\alpha$ -Synuclein assembles into higher-order multimers upon membrane binding to promote SNARE complex formation. *PNAS* 2014, 111, E4274–E4283.
- [29] Emamzadeh, F. N. Alpha-synuclein structure, functions, and interactions. *Journal of Research in Medical Sciences* 2016, 21:29.

- [30] H.J. Lee, S. L., C. Choi Membrane-bound alpha-synuclein has a high aggregation propensity and the ability to seed the aggregation of the cytosolic form. *J. Biol. Chem.* **2002**, *277*, 671–678.
- [31] Burre, J. The Synaptic Function of  $\alpha$ -Synuclein. *Journal of Parkinson's Disease* **2015**, *5*, 699–713.
- [32] Ueda, K.; Fukushima, H.; Maslah, E.; Xia, Y.; Iwai, A.; Yoshimoto, M.; Otero, D. A.; Kondo, J.; Ihara, Y.; Saitoh, T. Molecular cloning of cDNA encoding an unrecognized component of amyloid in Alzheimer disease. *Proceedings of the National Academy of Sciences* **1993**, *90*, 11282–6.
- [33] Fusco, G.; Simone, A. D.; Gopinath, T.; Vostrikov, V.; Vendruscolo, M.; Dobson, C. M.; Veglia, G. Direct observation of the three regions in  $\alpha$ -synuclein that determine its membrane-bound behaviour. *Nature Communications* **2014**, *5*.
- [34] Zarbiv, Y.; Simhi-Haham, D.; Israeli, E.; Elhadi, S. A.; Grigoletto, J.; Sharon, R. Lysine residues at the first and second KTKEGV repeats mediate  $\alpha$ -Synuclein binding to membrane phospholipids. *Neurobiol. Dis* **2015**, *70*, 90–98.
- [35] Vance, J. E. Phosphatidylserine and phosphatidylethanolamine in mammalian cells: two metabolically related aminophospholipids. *Journal of Lipid Research* **2008**, *49*, 1377–1387.
- [36] Lucki, N. C.; Sewer, M. B. Nuclear Sphingolipid Metabolism. *Annual Review of Physiology* **2012**, *74*, 131–151.
- [37] Palmano, K.; Rowan, A.; Guillermo, R.; Guan, J.; McJarrow, P. The Role of Gangliosides in Neurodevelopment. *Nutrients* **2015**, *7*, 3891–3913.
- [38] Huang, M.; Wang, B.; Li, X.; Fu, C.; Wang, C.; Kang, X.  $\alpha$ -Synuclein: A Multifunctional Player in Exocytosis, Endocytosis, and Vesicle Recycling. *Front. Neurosci.* **2019**, *13*.
- [39] Caraveo, P. K. A. G.; Lindquist, S.  $\alpha$ -Synuclein: Membrane Interactions and Toxicity in Parkinson's Disease. *Annu. Rev. Cell Dev. Biol.* **2010**, *273*, 211–233.
- [40] Hellstrand, E.; Grey, M.; Ainalem, M. L.; Ankner, J.; Forsyth, V. T.; Fragneto, G.; Haertlein, M.; Dauvergne, M. T.; Nilsson, H.; Brundin, P.; Linse, S.; Nylander, T.; Sparr, E. Adsorption of  $\alpha$ -synuclein to supported lipid bilayers: positioning and role of electrostatics. *ACS Chem. Neurosci.* **2013**, *4*, 1339–1351.
- [41] Pfefferkorn, C.; Heinrich, F.; Sodt, A. J.; Maltsev, A.; Pastor, R.; Lee, J. Depth of  $\alpha$ -Synuclein in a Bilayer Determined by Fluorescence, Neutron Reflectometry, and Computation. *Biophysical Journal* **2012**, *102*, 613–621.
- [42] Jao, C. C.; Der-Sarkissian, A.; Chen, J.; Langen, R. Structure of membrane-bound  $\alpha$ -synuclein studied by site-directed spin labeling. *Proceedings of the National Academy of Sciences* **2004**, *101*, 8331–8336.
- [43] Galvagnion, C.; Buell, A. K.; Meisl, G.; Michaels, T. C. T.; Vendruscolo, M.; Knowles, T. P. J.; Dobson, C. M. Lipid vesicles trigger  $\alpha$ -synuclein aggregation by stimulating primary nucleation. *Nature Chemical Biology* **2015**, *11*, 229–234.
- [44] Galvagnion, C. The Role of Lipids Interacting with  $\alpha$ -Synuclein in the Pathogenesis of Parkinson's Disease. *Journal of Parkinson's Disease* **2017**, *7*, 433–450.
- [45] Grey, M.; Dunning, C. J.; Gaspar, R.; Grey, C.; Sparr, P. B. E.; Linse, S. Acceleration of  $\alpha$ -Synuclein Aggregation by Exosomes. *The Journal of Biological Chemistry* **2015**, *11*, 2969–2982.

- [46] Gaspar, R.; Pallbo, J.; Weininger, U.; Linse, S.; Sparr, E. Ganglioside lipids accelerate  $\alpha$ -synuclein amyloid formation. *Biochimica et Biophysica Acta - Proteins and Proteomics* **2019**, *1866*, 1062–1072.
- [47] Hellstrand, E.; Nowacka, A.; Topgaard, D.; Linse, S.; Sparr, E. Membrane Lipid Co-Aggregation with  $\alpha$ -Synuclein Fibrils. *PLoS One* **2013**, *8*.
- [48] van Maarschalkerweerd, A.; Vetri, V.; Langkilde, A. E.; Fodera, V.; Vestergaard, B. Protein/Lipid Coaggregates are Formed During  $\alpha$ -Synuclein-Induced Disruption of Lipid Bilayers. *Biomacromolecules* **2014**, *15*, 3643–3654.
- [49] Reynolds, N. P.; Soragni, A.; Rabe, M.; Verdes, D.; Liverani, E.; Handschin, S.; Riek, R.; Seeger, S. Mechanism of Membrane Interaction and Disruption by  $\alpha$ -Synuclein. *Journal of American Chemical Society* **2011**, *133*, 19366–19375.
- [50] Galvagnion, C.; Topgaard, D.; Makasewicz, K.; Buell, A. K.; Linse, S.; Sparr, E.; Dobson, C. M. Lipid Dynamics and Phase Transition within  $\alpha$ -Synuclein Amyloid Fibrils. *The Journal of Physical Chemistry Letters* **2019**, *10*, 7872–7877.
- [51] Gaspar, R.; Idini, I.; Carlström, G.; Linse, S.; Sparr, E. Transient Lipid-Protein Structures and Selective Ganglioside Uptake During  $\alpha$ -Synuclein-Lipid Co-Aggregation. *Frontiers in Cell and Developmental Biology* **2021**, *9*, 266.
- [52] Volles, M. J.; Lee, S.-J.; Rochet, J.-C.; Shtilerman, M. D.; Ding, T. T.; Kessler, J. C.; P. T. Lansbury, J. Vesicle Permeabilization by Protofibrillar  $\alpha$ -Synuclein: Implications for the Pathogenesis and Treatment of Parkinson's Disease. *Biochemistry* **2001**, *40*, 7812–7819.
- [53] Lashuel, H. A.; Hartley, D.; Petre, B. M.; Walz, T.; Jr, P. T. L. Neurodegenerative disease: Amyloid pores from pathogenic mutations. *Nature* **2002**, *418*, 291–291.
- [54] Chaudhary, H.; Stefanovic, A. N.; Subramaniam, V.; Claessens, M. M. A. E. Membrane interactions and fibrillization of  $\alpha$ -synuclein play an essential role in membrane disruption. *FEBS Letters* **2014**, *588*, 4457–4463.
- [55] Chaudhary, H.; Subramaniam, V.; Claessens, M. M. A. E. Direct Visualization of Model Membrane Remodeling by  $\alpha$ -Synuclein Fibrillization. *ChemPhysChem* **2017**, *18*, 1620 – 1626.
- [56] Buell, A. K.; Galvagnion, C.; Gaspar, R.; Sparr, E.; Vendruscolo, M.; Knowles, T. P. J.; Linse, S.; Dobson, C. M. Solution conditions determine the relative importance of nucleation and growth processes in  $\alpha$ -synuclein aggregation. *PNAS* **2014**, *111*, 7671–7676.
- [57] Fink, A. L. Factors Affecting the Fibrillation of  $\alpha$ -Synuclein, a Natively Unfolded Protein. *Springer New York* 265–285.
- [58] S.J.L, F. L. . B. Relationship between the atomic pair distributionfunction and small-angle scattering: implications formodeling of nanoparticles. *Acta Cryst A* **2009**, *65*, 232–239.
- [59] Glatter, O. *Scattering Methods and Their Application in Colloid and interface Science*; Elsevier, 2018.
- [60] Pedersen, J. Analysis of small-angle scattering data from colloids and polymer solutions: modeling and least-squares fitting. *Advances in Colloid and Interface Science* **1997**, *70*, 171–210.

- [61] Beaucage, G. Approximations Leading to a Unified Exponential/Power-Law Approach to Small-Angle Scattering. *J. Appl. Cryst.* **1995**, *28*, 717–728.
- [62] Beaucage, G. Small-Angle Scattering from Polymeric Mass Fractals of Arbitrary Mass-Fractal Dimension. *J. Appl. Cryst.* **1996**, *29*, 134–146.
- [63] Hammouda, B. Analysis of the Beaucage model. *J. Appl. Cryst.* **2010**, *43*, 1474–1478.
- [64] Debye, P. Zerstreung von Röntgenstrahlen. *Annalen der Physik* **1915**, *351*, 809–823.
- [65] Keeler, J. *Understanding NMR Spectroscopy, 2nd Edition*; Wiley, 2010.
- [66] Colliex, C. Seeing and measuring with electrons: Transmission electron microscopy today and tomorrow—An introduction. *Comptes Rendus Physique* **2014**, *15*, 101–109.
- [67] Adrian, M.; Dubochet, J.; Lepault, J.; McDowell, A. Cryo-electron microscopy of viruses. *Nature* **1984**, *308*, 32–36.
- [68] Kelly, S. M.; Jess, T. J.; Price, N. C. How to study proteins by circular dichroism. *Biochimica et Biophysica Acta* **2005**, *1751*, 119–139.
- [69] Palmadottir, T.; Malmendal, A.; Leiding, T.; Lund, M.; Linse, S. Charge Regulation during Amyloid Formation of  $\alpha$ Synuclein. *J Am Chem Soc* **2021**, *143*, 7777–7791.
- [70] Gaspar, R.; Meisl, G.; Buell, A. K.; Young, L.; Kaminski, C. F.; Knowles, T. P.; Sparr, E.; Linse, S. Secondary nucleation of monomers on fibril surface dominates  $\alpha$ -synuclein aggregation and provides autocatalytic amyloid amplification. *Q Rev Biophys* **2014**, *50*, e6.
- [71] Pogostin, B.; Linse, S.; Olsson, U. Fibril Charge Affects  $\alpha$ -Synuclein Hydrogel Rheological Properties. *Langmuir* **2019**, *35*, 16536–16544.
- [72] Galvagnion, C.; Brown, J. W. P.; Ouberaï, M. M.; Flagmeier, P.; Vendruscolo, M.; Buell, A. K.; Sparr, E.; Dobson, C. M. Chemical properties of lipids strongly affect the kinetics of the membrane-induced aggregation of  $\alpha$ -synuclein. *Proc. Natl. Acad. Sci. U.S.A.* **2017**, *113*, 7065–7070.
- [73] Martinez, Z.; Zhu, M.; Han, S.; Fink, A. L. GM1 Specifically Interacts with  $\alpha$ -Synuclein and Inhibits Fibrillation. *Biochemistry* **2007**, *46*, 1868–1877.
- [74] Perez, R.; Waymire, J. C.; Lin, E.; Liu, J. J.; Guo, F.; Zigmond, M. J. A role for alpha-synuclein in the regulation of dopamine biosynthesis. *J Neurosci* **2002**, *22*, 3090–3099.
- [75] Yu, S.; Zuo, X.; Li, Y.; Zhang, C.; Zhou, M.; Zhang, Y. A.; Ueda, K.; Chan, P. Inhibition of tyrosine hydroxylase expression in alpha-synuclein-transfected dopaminergic neuronal cells. *Neurosci Lett* **2004**, *367*, 34–39.
- [76] Mizuno, N.; Varkey, J.; Kegulian, N. C.; Hegde, B. G.; Cheng, N.; Langen, R.; Steven, A. C. Remodeling of Lipid Vesicles into Cylindrical Micelles by  $\alpha$ -Synuclein in an Extended  $\alpha$ -Helical Conformation. *J. Biol. Chem.* **2012**, *287*, 29301–29311.
- [77] Varkey, J.; Isas, J. M.; Mizuno, N.; Jensen, M. B.; Bhatia, V. K.; Jao, C. C.; Petrlova, J.; Voss, J. C.; Stamou, D. G.; Steven, A. C.; Langen, R. Membrane curvature induction and tubulation are common features of synucleins and apolipoproteins. *J. Biol. Chem.* **2010**, *285*, 32486–93.



- [78] Sharon, R.; Goldberg, M. S.; Bar-Josef, I.; Betensky, R. A.; Shen, J.; Selkoe, D. J. alpha-Synuclein occurs in lipid-rich high molecular weight complexes, binds fatty acids, and shows homology to the fatty acid-binding proteins. *PNAS* **2001**, *98*, 9110–5.
- [79] Adamczyk, A.; Kacprzak, M.; Kazmierczak, A. Alpha-synuclein decreases arachidonic acid incorporation into rat striatal synaptoneurosomes. *Folia Neuropathol* **2007**, *45*, 230–235.
- [80] Madine, J.; Doig, A. J.; Middleton, A. D. A study of the regional effects of alpha-synuclein on the organization and stability of phospholipid bilayers. *Biochemistry* **2006**, *45*, 5783–5792.
- [81] Butler, B.; Goodwin, S.; Saha, K.; Becker, J.; Sambo, D.; Davari, P.; Khoshbouei, H. Dopamine Transporter Activity Is Modulated by alpha-synuclein. *J Biol Chem* **2015**, *290*, P29542–29554.
- [82] Sparr, E.; Linse, S. Lipid-protein interactions in amyloid formation. *Biochim. Biophys. Acta Proteins Proteom.* **2019**, *1867*, 455–457.
- [83] Iyer, A.; Claessens, M. M. Disruptive membrane interactions of alpha-synuclein aggregates. *BBA - Proteins and Proteomics* **2019**, *1867*, 468–492.
- [84] Nakamura, K. et al. Direct Membrane Association Drives Mitochondrial Fission by the Parkinson Disease-associated Protein  $\alpha$ -Synuclein. *J. Biol. Chem.* **2011**, *286*, 20710–20726.
- [85] Meredith, G.; Totterdell, S.; Petroske, E.; Cruz, K. S.; Callison, R.; Lau, Y.-S. Lysosomal malfunction accompanies alpha-synuclein aggregation in a progressive mouse model of Parkinson's disease. *Brain Research* **2002**, *956*, 156–165.
- [86] Fujita, Y.; Ohama, E.; Takatama, M.; Al-Sarraj, S.; Okamoto, K. Fragmentation of Golgi apparatus of nigral neurons with  $\alpha$ -synuclein-positive inclusions in patients with Parkinson's disease. *Acta Neuropathol.* **2006**, *112*, 261–265.
- [87] Winner, B. et al. In vivo demonstration that  $\alpha$ -synuclein oligomers are toxic. *PNAS* **2011**, *108*, 4194–4199.
- [88] Karpinar, D. P. et al. Pre-fibrillar alpha-synuclein variants with impaired betastructure increase neurotoxicity in Parkinson's disease models. *EMBO J* **2009**, *28*, 3256–3268.
- [89] Danzer, K. M.; Haasen, D.; Karow, A. R.; Moussaud, S.; Habeck, M.; Giese, A.; Kretschmar, H.; Hengerer, B.; Kostka, M. Different Species of  $\alpha$ -Synuclein Oligomers Induce Calcium Influx and Seedings. *J Neurosci* **2007**, *27*, 9220 –9232.
- [90] Kumar, R.; Das, S.; Mohite, G.; Rout, S.; Halder, S.; Jha, N.; Ray, S.; Mehra, S.; Agarwal, V.; Maji, S. Cytotoxic Oligomers and Fibrils Trapped in a Gel-like State of  $\alpha$ -Synuclein Assemblies. *Angew. Chem. Int. Ed* **2018**, *57*, 5262–5266.
- [91] Daicic, J.; Fogdenv, A.; Carlsson, I.; Wennerstrom, H.; Jonsson, B. Bending of ionic surfactant monolayers. *Phys Rev E* **1996**, *54*, 3984–3998.
- [92] Maksewicz, K.; Wennmalm, S.; Stenqvist, B.; Fornasier, M.; Andersson, A.; Jönsson, P.; Linse, S.; Sparr, E. Cooperativity of  $\alpha$ -Synuclein Binding to Lipid Membranes. *ACS Chem. Neurosci.* **2021**, *12*, 2099–2109.
- [93] Cohen, A.; Calkins, E. Electron microscopic observations on a fibrous component in amyloid of diverse origins. *Nature* **1959**, *183*, 1202–1203.

- [94] Li, Y.; Zhao, C.; Luo, F.; Liu, Z.; Gui, X.; Luo, Z.; Zhang, X.; Li, D.; Liu, C.; Li, X. Amyloid fibril structure of  $\alpha$ -synuclein determined by cryo-electron microscopy. *Cell Res.* **2018**, *28*, 897–903.
- [95] Vilar, M.; Chou, H. T.; Luhrs, T.; Maji, S. K.; Riek-Loher, D.; Verel, R.; Manning, G.; Stahlberg, H.; Riek, R. The fold of  $\alpha$ -synuclein fibrils. *PNAS* **2008**, *105*, 8637–8642.
- [96] Tuttle, M. D. et al. Solid-state NMR structure of a pathogenic fibril of full-length human  $\alpha$ -synuclein. *Nat. Struct. Mol. Biol.* **2016**, *23*, 409–415.
- [97] Li, B.; Ge, P.; Murray, K. A.; Sheth, P.; Zhang, M.; Nair, G.; Sawaya, M.; Shin, W.; Boyer, D. R.; Ye, S.; Eisenberg, D. S.; Zhou, Z. H.; Jiang, L. Cryo-EM of full-length  $\alpha$ -synuclein reveals fibril polymorphs with a common structural kernel. *Nat. Commun.* **2018**, *9*.
- [98] Guerrero-Ferreira, R. et al. Two new polymorphic structures of human full-length alpha-synuclein fibrils solved by cryo-electron microscopy. *eLife* **2019**, *9*, e48907.
- [99] Shults, C. W. Lewy Bodies. *PNAS* **2006**, *103*, 1661–1668.
- [100] Olanow, C. W.; Perl, D. P.; DeMartino, G. N.; McNaught, K. S. P. Lewy-body formation is an aggresome-related process: a hypothesis. *Lancet Neurol.* **2004**, *3*, 496–503.
- [101] Duffy, P.; Tennyson, V. Phase and electron microscopic observations of Lewy bodies and melanin granules in the substantia nigra and locus caeruleus in Parkinson's disease. *J. Neuropathol. Exp. Neurol.* **1965**, *24*, 398–414.
- [102] Forno, L. S.; Norville, R. L. Ultrastructure of Lewy Bodies in the Stellate Ganglion. *Acta neuropath.* **1976**, *34*, 183–197.
- [103] Croke, R. L.; Patil, S. M.; Quevreaux, J.; Kendall, D. A.; Alexandrescu, A. T. NMR determination of pKa values in  $\alpha$ -synuclein. *Protein Science* **2011**, *20*, 256–269.
- [104] M.J., S.; P.T., S. Microstructural regimes of colloidal rod suspensions, gels, and glasses. *Soft Matter* **2010**, *6*, 1391–1400.
- [105] Serpell, L.; Berriman, J.; Jakes, R.; Goedert, M.; Crowther, R. A. Fiber diffraction of synthetic  $\alpha$ -synuclein filaments shows amyloid-like cross- $\beta$  conformation. *Proceedings of the National Academy of Sciences* **2000**, *97*, 4897–4902.
- [106] Rodriguez, J. et al. Structure of the toxic core of  $\alpha$ -synuclein from invisible crystals. *Nature* **2015**, *525*.



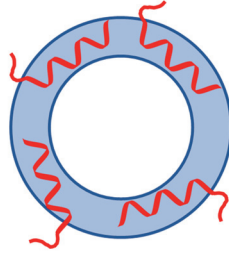


# Scientific Publications



## Part I

**Overarching question:** What is the nature of the interaction between monomeric aSyn and lipid membranes and does the fibril formation in the presence of lipid membranes lead to a protein-lipid co-assembly formation and membrane disruption?



An illustration of a vesicle (blue) covered with aSyn monomers (red) that assume an  $\alpha$ -helical conformation upon the adsorption on the vesicle surface.